Chemical Geology 724 (2026) 123707

Contents lists available at ScienceDirect

Chemical Geology

journal homepage: www.elsevier.com/locate/chemgeo

Research Paper

The late shoulder season modifies the mobility of iron and dissolved organic carbon in rivers from distinct permafrost regions

Maëlle Villani [a,*], Catherine Hirst [b], Eléonore du Bois d'Aische [a], Cécile Osy [a], Maxime Thomas [a], Philippe Roux [a], Erik Lundin [c], Justin Ledman [d], Edward A.G. Schuur [d], Sophie Opfergelt [a]

[a] Earth and Life Institute, Université catholique de Louvain, Louvain-la-Neuve, Belgium
[b] Department of Earth Sciences, Durham University, Durham, United Kingdom
[c] Abisko Scientific Research Station, Swedish Polar Research Secretariat, Abisko, Sweden
[d] Center for Ecosystem Science and Society, Northern Arizona University, Flagstaff, AZ, USA

ARTICLE INFO

Editor: Oleg Pokrovsky

Keywords:
Arctic
River
Iron
Dissolved organic carbon
Late shoulder season

ABSTRACT

Rivers are important suppliers of iron (Fe) and dissolved organic carbon (DOC) from land to sea. While elemental transport in Arctic rivers has been studied mainly during summer, their mobility during the late shoulder season (i.e., the transition between the end of summer and the beginning of winter) remains poorly constrained. Here, we investigate how Fe and DOC mobility evolve during the late shoulder season in two rivers from distinct permafrost regions and hydrological conditions (in Alaska, USA and Abisko, Sweden). Iron and DOC were characterized using their concentrations, percentage of colloidal Fe, and indirect Fe-oxides tracers (Ce anomaly and δ^{30}Si). We show two contrasting processes: (i) in Alaska, progressive river ice formation coincides with a shift toward groundwater-dominated river input, suggesting aggregation of Fe as particles (>0.22 μm), evidenced by a decrease in Fe concentrations in the filtered water (<0.22 μm) over the late shoulder season; the concurrent higher negative Ce anomaly, and the decrease in DOC concentrations, further suggest the aggregation of particulate Fe-oxides associated with DOC; (ii) in Abisko, warmer and near-stagnant river conditions sustain soil pore water-river connectivity over the late shoulder season, enabling lateral transfer of Fe, evidenced by increase Fe concentrations; the increase in the percentage of colloidal Fe, the lower negative Ce anomaly, the slight decrease in δ^{30}Si, and the increase in DOC concentrations, further suggest an increase in colloidal Fe-oxides associated with DOC (1 nm- 0.22 μm) in the river. These contrasting Fe size ranges have direct implications for Arctic DOC export.

1. Introduction

Rivers are important suppliers of iron (Fe) and dissolved organic carbon (DOC) from land to sea (Dai and Martin, 1995; Hirst et al., 2023a; Krachler et al., 2005, 2010; Kritzberg et al., 2014). Iron is transported largely as particles (> 0.22 μm) and colloids (1 nm - 0.22 μm), particularly comprising chemically reactive Fe (oxyhydr)oxides (e.g., ferrihydrite) as Fe-oxides associated with DOC (Hirst et al., 2017; Pokrovsky and Schott, 2002; Pryer et al., 2020). A remaining Fe fraction is transported as truly dissolved Fe (< 1 nm), commonly as aqueous species (Fe(*II*)aq, Fe(*III*)aq) or low-molecular-weight Fe-DOC complexes (Ilina et al., 2014). Associations between Fe-oxides and DOC are particularly important because Fe-oxides physico-chemically stabilize DOC against microbial degradation in soil pore water (Kappler et al., 2021; Kleber et al., 2021; Opfergelt, 2020; Opfergelt et al., 2026). Once transferred to aquatic systems, this DOC can then either (i) be stabilised by mineral elements, aggregate and contribute to aquatic sediments for a delayed onset of greenhouse gases release or (ii) breakdown (photo or microbially mediated degradation) for immediate contribution to emissions as greenhouse gases (CO_2 and CH_4; Bowen et al., 2020; Hirst et al., 2017; Kelley et al., 2026). Decomposition of DOC in aquatic systems is primarily governed by light availability, temperature, and dissolved oxygen concentrations, which together control both photodegradation and microbial mineralization rates (Chupakova et al., 2018; Grunert et al., 2021). However, Fe represents an additional and important modulator of DOC mobility: Fe-oxides associated with DOC in rivers represent a key

* Corresponding author.
E-mail address: maelle.villani@uclouvain.be (M. Villani).

https://doi.org/10.1016/j.chemgeo.2026.123707
Received 24 June 2026; Received in revised form 3 September 2026; Accepted 11 September 2026
Available online 11 September 2026

control on whether this carbon is retained or mineralized (Opfergelt et al., 2026). As permafrost soils store more than 1600 Gt of OC, approximately twice the amount currently present in the Earth's atmosphere (Strauss et al., 2025), and DOC lateral fluxes from permafrost regions account for approximately 5% of the permafrost carbon pool exported annually by hydrological processes (Plaza et al., 2019), understanding the mechanisms controlling DOC stabilization and mobilization is critical (Drake et al., 2018; Tank et al., 2018). Under a climate scenario without mitigation, nearly 70% of near-surface permafrost is projected to thaw by 2100 (Hugelius et al., 2014; Schuur et al., 2022), intensifying water circulation and discharge to major river networks (Tian et al., 2026; Walvoord et al., 2012), and increasing the transfer of dissolved elements such as Fe and DOC to Arctic aquatic systems (Dial et al., 2026). Whether exported DOC reaches the ocean as mineral-associated forms or/and is rapidly mineralized in rivers therefore has major implications for the permafrost carbon feedback.

Understanding the mobility of Fe and DOC requires knowing how hydrological connectivity evolves through time, as soil pore waters and groundwaters represent the primary source of water and constituents exported to inland and coastal aquatic systems (Vonk et al., 2019). Moreover, element transport in Arctic rivers has been predominantly studied during spring floods or at the year scale (Krickov et al., 2019; Sun et al., 2018), while transitional periods such as the late shoulder season (i.e., the transition between the end of summer and the beginning of winter) remain poorly constrained (Shogren et al., 2020). This knowledge gap regarding the late shoulder season is particularly concerning given that the strongest climate amplification occurs during these late shoulder and winter seasons (Box et al., 2019), when hydrological connectivity and its consequences on Fe and DOC are least understood (Lyu et al., 2024; Natali et al., 2019). Furthermore, multi-site comparisons are currently lacking to resolve how environmental conditions during this late shoulder season vary across permafrost regions (Krickov et al., 2020; Villani et al., 2025; Vonk et al., 2019; Walvoord et al., 2019).

To fill this gap, this study addresses the following research question: how does the mobility of Fe and DOC evolve during the late shoulder season in Arctic rivers from distinct permafrost regions? River waters ($<$ 0.22 μm) were collected from discontinuous permafrost regions in Alaska, USA (Panguingue Creek), and from a sporadic permafrost region in Abisko, Sweden (Stordalen Mire) during the late shoulder season (September–November 2023 in Alaska and 2021 in Abisko; Fig. 1).

These samples are used to address two successive sub-objectives derived from the research question. Firstly, we need to assess hydrological connectivity during the late shoulder season by identifying water inputs in the rivers using pH, conductivity, and stable water isotopes ($\delta^{18}O$ and δD). Stable water isotopes represent a powerful proxy to trace these shifting water sources between soil pore waters and deep groundwaters (Mueller et al., 2014; Tan et al., 2016; Tananaev et al., 2021). Water inputs in the rivers, coming from soil pore waters or/and deep groundwaters, will impact the mobility of Fe and DOC in the rivers.

Secondly, we need to assess the change in Fe and DOC concentrations in the rivers with the changes in hydrological connectivity along the late shoulder season. We hypothesize that the changing conditions along the late shoulder season can lead to the formation of Fe-oxides in river water; this is why we assess the percentage of colloidal Fe and we use water Ce anomaly (Ce/Ce*) as an indirect tracer to identify the presence of Fe-oxides (see Section 2.4.5). We also use water silicon isotopic composition ($\delta^{30}Si$) as an indirect tracer to support the presence of Fe-oxides (Delstanche et al., 2009; see Section 2.4.6). Together with direct measurements of colloidal Fe, Ce anomalies and $\delta^{30}Si$ provide complementary indirect constraints on the formation of Fe-oxides.

Ultimately, the evolution of the Fe-oxides occurrence and DOC concentration in river water along the late shoulder season is used to inform on the mobility of Fe and DOC, and more specifically on the potential role of Fe in mediating DOC transport.

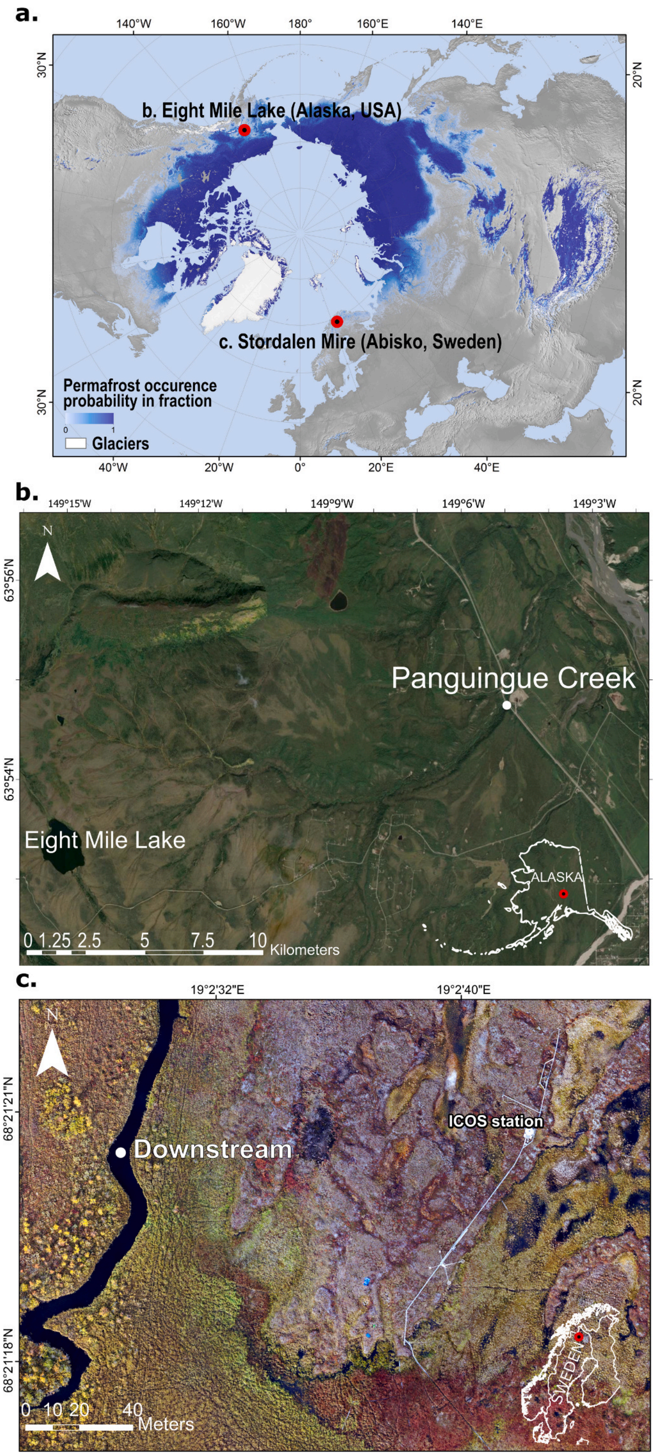

Fig. 1. Permafrost area in the Northern Hemisphere with Eight Mile Lake (Alaska, USA) and the Stordalen Mire (Abisko, Sweden) as red dots (**a.**; Obu et al., 2019). Sampling locations of river waters collected at Panguingue Creek near Eight Mile Lake, Alaska (**b.**) and downstream of the study site at the Stordalen Mire, Abisko (**c.**). (For interpretation of the references to colour in this figure legend, the reader is referred to the web version of this article.)

2. Materials and methods

2.1. Study sites

Field campaigns took place in two different geographic zones: the Panguingue Creek catchment (63° 52′ N, 149° 15′ W; 700 m a.s.l), in

Alaska, USA, and at the Stordalen Mire (68° 20′ N, 19° 03′ E; 385 m a.s.l.) in Abisko, Sweden (Fig. 1a; Obu, 2021). These two field campaigns were conducted during the late shoulder season, between September and November (2023 in Alaska and 2021 in Abisko).

In Alaska, river waters were sampled near Eight Mile Lake at the Panguingue Creek river (second-order stream) from the Panguingue Creek catchment (66 km^2) between September 17 to October 25, 2023 (Fig. 1b). This catchment is in a discontinuous permafrost region (50–90% aerial permafrost extent) and has moist acidic tundra soils, classified as Cryosols (WRB), with an organic layer of 45–65 cm thick (> 20% OC) which covers cryoturbated mineral soil (< 20% OC) that is a mixture of glacial till (small stones and cobbles) and windblown loess (Natali et al., 2011). The active layer thickness is between 50 and 120 cm (Kelley et al., 2021). Its geology is composed of Tertiary sedimentary rocks, overlain by gravelly glacial till and aeolian silt including the Pliocene Nenana gravel (Soil Survey Staff, 1999). Vegetation is composed of the sedges such as *E. vaginatum*, shrubs such as *Betula nana*, and mosses such as *Sphagnum* sp. The mean annual temperature in Healy is −2.87 °C (2013−2023), with seasonal means ranging from −9.9 °C (October–April) to 6.9 °C (May–September; Kennedy et al., 2026). Mean annual precipitation (rain and snow) is 391 mm. Snow cover, present from mid-September to mid-May, averages 52 cm in depth (Natali et al., 2012; Osterkamp et al., 2009; Vogel et al., 2009). The Panguingue Creek river exhibits a seasonal discharge variability, from 5 $m^3 s^{-1}$ during spring freshet in May down to a base flow of 0.2 $m^3 s^{-1}$ during summer months (Kelley et al., 2025). The Panguingue Creek catchment drains from water tracks and soil pore waters at higher elevation (670 m) into first-order streams that converge into the studied second-order Panguingue Creek river (412 m at the catchment outlet), with an average slope of 2.3° between the pore water sampling sites and the second-order stream, consistent with a free-flowing river (Kelley et al., 2025).

In Abisko, river waters were sampled at the downstream river (first-order stream) at the Stordalen Mire (15 km^2), a sporadic permafrost region (10–50% aerial permafrost extent), between September 15 to November 11, 2021 (Fig. 1c). The Stordalen mire is located approximately 10 km east of the village of Abisko, in the lower part of a catchment that drains into Lake Torneträsk (Olefeldt and Roulet, 2012). The formation of peat in Stordalen Mire started more than 5000 years ago, and the peat layer had a mean thickness of 0.5 m in 2009 (Klaminder et al., 2009). As a sporadic permafrost region, the active layer thickness is between 50 cm and more than 200 cm depth (Aische et al., 2025; Thomas et al., 2025). The geology of the Stordalen catchment is predominantly granites and metamorphic rocks with lesser sedimentary equivalents present (Selinus et al., 2001). Till, silt and peat, classified as Histosols and Cryosols (WRB), are the main soil types developed above the bedrock (Åkerman and Johansson, 2008; Mzobe et al., 2020). Vegetation is composed of dwarf shrubs, e.g., *E. hermaphroditum*, but also sedges such as *C. rostrate*, *E. angustifolium* and *E. vaginatum,* and mosses such as *Sphagnum* sp. (Åkerman and Johansson, 2008). The mean annual air temperature in Abisko is 0.87 °C (2013–2023) with seasonal means ranging from −4.2 °C (October–April) to 9.1 °C (May–September), and the mean annual precipitation (rain and snow) is 329 mm (SMHI, 2026). At Stordalen Mire, the river is characterized by very low discharge, averaging around 0.14 $m^3 s^{-1}$ (Mzobe et al., 2018; Olefeldt et al., 2013). The river drains through the mire before discharging toward Lake Torneträsk. This low, stable discharge, combined with the near-flat gradient of the lower catchment (Klaminder et al., 2009), leaves the river as a near-stagnant river rather than a free-flowing river (Olefeldt and Roulet, 2012).

2.2. Air temperature

In Alaska and Abisko, the air temperature was monitored continuously between September 17 and November 11 using ZL6 Pro Data Logger connected to TEROS-12 (Meter) probes with a temporal resolution of 10 min in Abisko, and one hour in Alaska.

2.3. River water sampling

River waters in Alaska (n = 11) and Abisko (n = 17) were collected every three days during the field campaigns. For each water sample, a small volume was kept unfiltered for water isotopes measurement. At both sites, water was filtered at 0.70 μm with glass fiber filters (pre-combusted at 450 °C) to measure the DOC concentration, and at 0.22 μm with cellulose acetate filters to measure Fe, La, Ce, Pr, and Si concentrations, and δ^{30}Si. Pore size tests for DOC (0.45 μm with glass fiber filters pre-combusted at 450 °C) and Fe (0.40 μm with cellulose acetate) were carried out in order to compare DOC (0.70 μm) and Fe (0.22 μm) concentrations, with 0.08% difference between 0.70 μm and 0.45 μm for DOC, and 10% difference between 0.22 μm and 0.45 μm for Fe (Fig. S1).

The proportion of Fe-bearing colloids (percentage of colloidal Fe) in both rivers was obtained by a second step of filtration on the 0.22 μm filtered river waters. In Alaska, river waters were filtered using a stirred ultrafiltration cell (Amicon®, 50 mL) under a constant pressure mode of 500 kPa provided by pressurized nitrogen gas (Ultracel® regenerated cellulose) with a molecular weight cut-off size of 1 kDa (∼1.3 nm). In Abisko, river waters were separated using tubular dialysis membranes (Spectrapore 7®) with a molecular weight cut-off size of 1 kDa (Hirst et al., 2022; Vasyukova et al., 2012). For each sample in Abisko, the clean membrane was filled with 50 mL of MilliQ® water, and was placed into an acid-washed 2 L bottle containing unfiltered river water for 72 h. Both methods provided the operationally defined fraction of ∼1 nm – 0.22 μm.

2.4. Chemical analyses

2.4.1. pH, electrical conductivity, and water temperature measurements

At both river sites (n = 28), the pH, electrical conductivity (μS cm^{-1}; conductivity in the text), and water temperature were directly measured in the field using a probe from HANNA Instruments (HI991300). Data from Abisko were published in Villani et al. (2025).

2.4.2. Water isotopes measurements

At both river sites (n = 28), oxygen (δ^{18}O) and deuterium (δD) isotopes values (Fig. S2) were determined on unfiltered river water using Cavity Ring Down Spectroscopy on a Liquid Water Isotope Analyzer (L2130-i, Picarro®). Values are normalized between VSLAP and VSMOW and reported in per mil deviation relative to VSMOW. The accuracy was ±0.5% for δ^{18}O and ± 0.7% for δD and was assessed using the reference material USGS47 (n = 7). The reproducibility was ±0.5‰ for δ^{18}O and ± 0.6‰ for δD. The blank samples (n = 6) were on average − 7.00 ± 0.19‰ for δ^{18}O, and − 48.82 ± 0.58‰ for δD.

2.4.3. Dissolved organic carbon concentration measurements

For both river sites (n = 28), DOC concentration in river waters was measured using high-temperature catalytic oxidation (Shimadzu® TOC-VCPH). The detection limit was 0.1 mg L^{-1} and the accuracy was ±5% using a standardized water 10 ppm DOC. The reproducibility was ±2%. The blank samples (n = 18) were on average 0.044 ± 0.071 mg L^{-1}. Data from Abisko were published in Villani et al. (2025).

2.4.4. Iron concentration and percentage of colloidal iron

For both river sites (n = 28), Fe concentration was measured in river waters filtered at 0.22 μm, and in the ultrafiltrated (Alaska) and dialysis (Abisko) fractions (n = 28) by an inductively coupled plasma-optical emission spectrometer (ICP-OES, iCAP 6500 ThermoFisher Scientific). The accuracy was ±2% and was assessed using the water reference material SLRS-4 (Yeghicheyan et al., 2001). The reproducibility was ±0.3%. The detection limit was 0.001 mg L^{-1}. The blank samples (n = 8) were on average 0.010 ± 0.009 mg L^{-1}. The percentage of colloidal Fe in river waters (fraction from ∼1 nm to ∼0.22 μm) was obtained by difference between measurements on these two different size fractions of the water (< 0.22 μm and < 1 kDa). Data from Abisko were published in Villani et al. (2025).

2.4.5. Cerium anomaly measurements

Cerium (Ce) is a redox-sensitive rare earth element whose tetravalent form (Ce^{4+}) preferentially adsorbs onto Fe-oxides, resulting in negative Ce anomalies in the filtered fraction (< 0.22 μm) when Fe oxides are predominantly present as particles (> 0.22 μm; Catrouillet et al., 2019; Davranche et al., 2016; Pourret et al., 2008, 2009). Conversely, when Fe-oxides are present as colloids (between 1 nm and 0.22 μm), Ce^{4+} remains within the filtered fraction alongside the Fe-oxide colloids, resulting in a less negative Ce anomaly. The Ce anomaly thus indirectly tracks the size range and abundance of Fe-oxide phases in river waters, making it a sensitive indirect tracer for Fe-oxides independently of total Fe concentration measurements.

To calculate the Ce anomaly, La, Ce, and Pr concentrations were measured at both sites using ICP-MS (iCAP Q ICP-MS, Thermo Fisher Scientific, Waltham, MA, USA) in river waters ($n = 28$) and soil pore waters ($n = 515$; in Supplementary). The detection limit for La, Ce, and Pr concentrations were 0.005, 0.0005, and 0.0005 μg L^{-1} respectively. The accuracies on element concentrations (± 6% for La, ± 4% for Ce, and ± 4% for Pr) were assessed using the water reference material SLR S-6 (Yeghicheyan et al., 2001). The reproducibility for La, Ce, and Pr was ±1%. The blank samples ($n = 4$) for La, Ce, and Pr were on average 0.00002 ± 0.00005 μg L^{-1}, 0.00005 ± 0.00004 μg L^{-1}, and 0.000001 ± 0.000004 μg L^{-1}.

The concentrations of La, Ce, and Pr were normalized based on UCC (La_{UCC}, Ce_{UCC}, Pr_{UCC}; upper continental crust; Rudnick and Gao, 2003), which is almost identical to data from Swedish till (Conrad et al., 2024; Öhlander et al., 1996). The Ce anomaly (Ce/Ce*), called "negative" if the result is <1 and "positive" if the result is >1 (Fig. S3), compared to UCC and the neighboring elements. The Ce anomaly (Ce/Ce*) was then calculated as:

$$\frac{Ce}{Ce^{*}} = \frac{Ce_{UCC}}{\frac{1}{2}\, x\, (La_{UCC} + Pr_{UCC})}$$

2.4.6. Silicon concentration and silicon isotope analysis

For both river sites ($n = 28$), Si concentration was measured in river waters filtered at 0.22 μm by an inductively coupled plasma-optical emission spectrometer (ICP-OES, iCAP 6500 ThermoFisher Scientific). The detection limit was 0.002 mg L^{-1}. The accuracy was ±0.8% and was assessed using the water reference material SLRS-4 (Yeghicheyan et al., 2001). The reproducibility was ±0.3%. The blank samples ($n = 8$) were always below the detection limit. Data from Abisko were published in Villani et al. (2025).

Silicon isotopes can be used as an indirect tracer to support the presence of Fe-oxides (Delstanche et al., 2009). More specifically, light silicon isotopes preferentially bind to Fe-oxides, leading to an increase in $\delta^{30}Si$ in the filtered river fraction (< 0.22 μm) when Fe-oxides are predominantly present as particles (> 0.22 μm). For both river sites ($n = 28$), the silicon isotopic composition ($\delta^{30}Si$) was measured in river waters using a MC-ICP-MS (Neptune Plus™ High Resolution Multicollector ICP-MS, Thermo Fisher Scientific, Earth & Life Institute, UCLouvain, Belgium) following the same method than Hirst et al. (2023b). Sample preparation was done in clean lab conditions (ISO 6) under a laminar flow hood (ISO 5). A volume equivalent to 10 μg Si was dried down. The dissolved organic carbon in solution was removed by repeated cycles of heating (60 °C) with concentrated HNO_3 and H_2O_2 and evaporating (80 °C) cycles (Hughes et al., 2011). After repeated cycles, the sample was digested in 0.125 M NaOH for four hours at 100 °C, then acidified with HNO_3. Silicon was purified from the matrix with a one-stage column chemistry using a cation exchange resin (Biorad AG50W-X12; Georg et al., 2006). The Si recovery was 94.5 ± 5.4% and Na^{+} concentrations below the detection limit following column chemistry. Blank samples ($n = 6$) were finally measured after purification to prevent Si contamination and concentrations were all below the detection limit.

The silicon isotopic composition ($\delta^{30}Si$) was measured by MC-ICP-MS in wet plasma mode in high resolution ($\Delta m/m \approx 9000$) using a PFA nebulizer of 100 μL min^{-1} uptake rate. The instrumental mass bias was corrected using the standard-sample bracketing technique and an external Mg doping (Cardinal et al., 2003). The analyses were performed in 2% HNO_3 matrix, with a typical sensitivity of 3.5 V for 1 mg L^{-1} Si and an instrumental blank <30 mV. The $\delta^{30}Si$ compositions are expressed in relative deviations of $^{30}Si/^{28}Si$ ratio from an in-house standards (Quartz Merck) isotopically similar to NBS28 reference standard using the common δ-notation (‰) as follows (Abraham et al., 2008): $\delta^{30}Si = [(^{30}Si/^{28}Si)_{sample}/(^{30}Si/^{28}Si)_{Quartz\ Merck} - 1] \times 1000$. The long-term precision and accuracy of the MC-ICP-MS was assessed from diatomite standard measurements ($\delta^{30}Si = 1.29 \pm 0.05$‰, SD; $n = 7$) which are consistent with previously reported values ($\delta^{30}Si = 1.26 \pm 0.10$‰; Reynolds et al., 2007). Data from Abisko were published in Villani et al. (2025).

2.5. Data treatment

Values are reported as mean ± standard deviation throughout the manuscript. All graphs and statistics were performed using R 4.0.2 (RStudio Inc., Boston, Massachusetts, USA) and plots using the ggplot2 package. The significant differences in temperature were evaluated using a non-parametric Wilcoxon test. The significant trend in pH, conductivity, water isotopes, DOC and Fe concentrations, percentage of colloidal Fe, Ce anomaly, Si concentration, and Si isotopes over the late shoulder season were evaluated using a non-parametric Mann-Kendall test. Kendall'tau shows trend direction (positive = increasing, negative = decreasing) and its magnitude reflects trend strength. The 95% confidence intervals of the statistic were used to test for significant differences or trends, equivalent to a ***p***-value cutoff of 0.05.

3. Results and discussion

3.1. Contrasting climatic regimes across two permafrost regions during the late shoulder season

In this study, two sites of distinct permafrost regions are compared: discontinuous in Alaska and sporadic in Abisko. Beyond their permafrost extent, the two sites also differ hydrologically: the river in Alaska has pronounced seasonal discharge variability, while the river in Abisko behaves more like a near-stagnant river than a free-flowing river (see Section 2.1). During the late shoulder season, mean air temperature in Alaska (−3.5 ± 5.4 °C) is significantly lower by 5 °C (Wilcoxon test; ***p***-value <0.05) than in Abisko (2.0 ± 5.2 °C; Fig. 2a,c). Although the two sites were sampled in different years (2023 in Alaska and 2021 in Abisko), this thermal contrast primarily reflects site-specific climatic differences rather than interannual variability. This is supported by Arctic temperature rankings, with 2021 being the 12th warmest year since 1950 and 2023 the 6th warmest (Copernicus, European State of the Climate), indicating that Abisko remained warmer than Alaska despite being sampled during a comparatively colder Arctic year. Precipitation patterns also differ between the two sites: Alaska shows sparse and generally low-amplitude events throughout the sampling period, whereas Abisko experiences more frequent precipitation, including a marked event of about 15 mm in late October (Fig. 2a,c). These environmental conditions result in differences in river water temperatures in Alaska and in Abisko during the late shoulder season (Fig. 2b,d): river water temperatures significantly decrease from 5.6 to 0.1 °C in Alaska and from 9.5 to 0.6 °C in Abisko (Mann-Kendall test; ***p***-value <0.05; Tables S1-S2). In addition to water temperature, change in river ice cover may also influence river chemical composition such as dissolved oxygen and redox potential (Chambers et al., 2000). Together, these contrasting geographic, climatic and hydrological conditions, are likely to drive distinct hydrological connectivity patterns between the two sites during the late shoulder season, with cascading effects on the

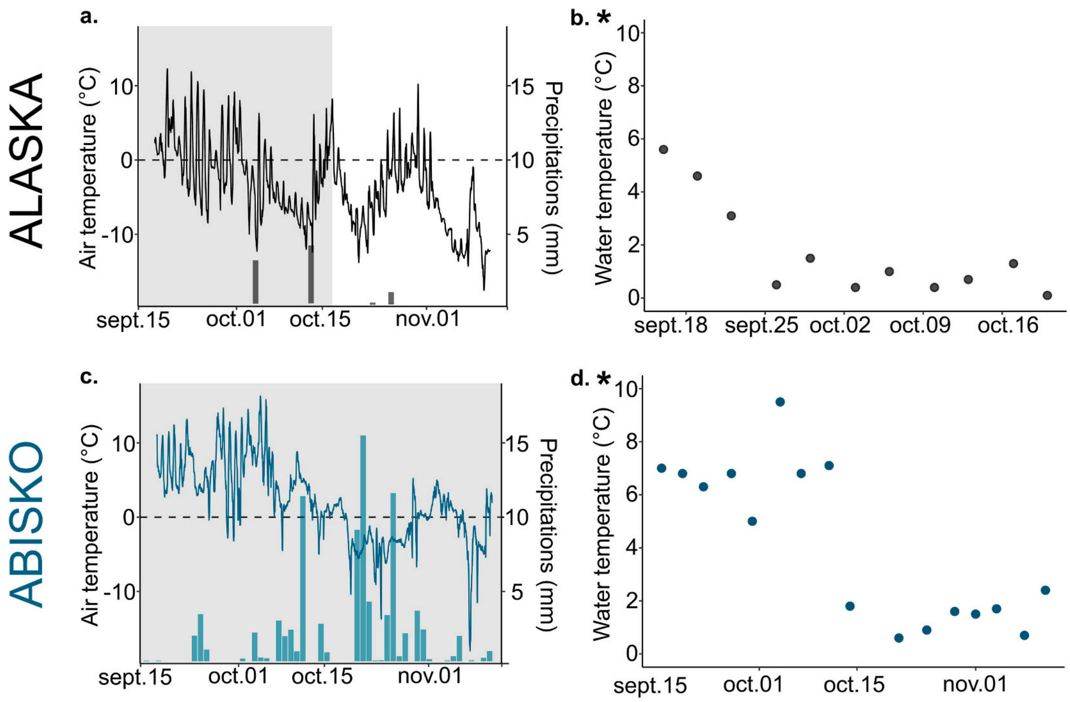

Fig. 2. Air temperature (°C) and precipitations (rain and snow; from SMHI and Kennedy et al., 2026; mm) from September 17 to November 11 in Alaska (**a.**; in black; in 2023) and in Abisko (c.; in blue; in 2021); river water temperature (°C) during the water sampling in Alaska from September 17 to October 25, 2023 (b.) and in Abisko from 15 September to 11 November 2021 (d.). The shaded area represents the water sampling period. Mann-Kendall test was performed to identify significant temporal trends in river water temperatures (* if *p*-value <0.05; Tables S1-S2). Air temperature from Abisko was published in Villani et al. (2025). (For interpretation of the references to colour in this figure legend, the reader is referred to the web version of this article.)

mobility of Fe and DOC.

3.2. Hydrological connectivity under contrasting geographic, climatic and hydrological regimes

In river waters from Alaska, pH values, conductivity, oxygen isotopes ($\delta^{18}O$) and deuterium isotopes (δD) are 7.88 ± 0.08, 231 ± 33 μS cm^{-1}, −18.65 ± 0.13‰, and − 145.95 ± 1.18‰ respectively (Fig. 3a-d; Table S1). Over the late shoulder season, there is no significant change in pH, but conductivity increases significantly (by a factor of 1.5), and $\delta^{18}O$ and δD values decrease significantly by 0.38‰ and 3.37‰, respectively (Mann-Kendall test; ***p***-value <0.05; Table S1). The decrease in $\delta^{18}O$ could be induced by a relative increase in deep groundwater flow path inputs (Juhls et al., 2020; O'Donnell et al., 2012; Putman et al., 2019). These deep groundwaters have lower $\delta^{18}O$ values than surface soil pore water (Hirst et al., 2022; Roux et al., 2026). In addition to their distinct isotopic signature, groundwaters generally exhibit higher conductivity than shallow soil pore waters because longer residence times, that enhance water–mineral interactions within deeper mineral horizons, lead to greater solute accumulation (Cochand et al., 2019; Diak et al.,

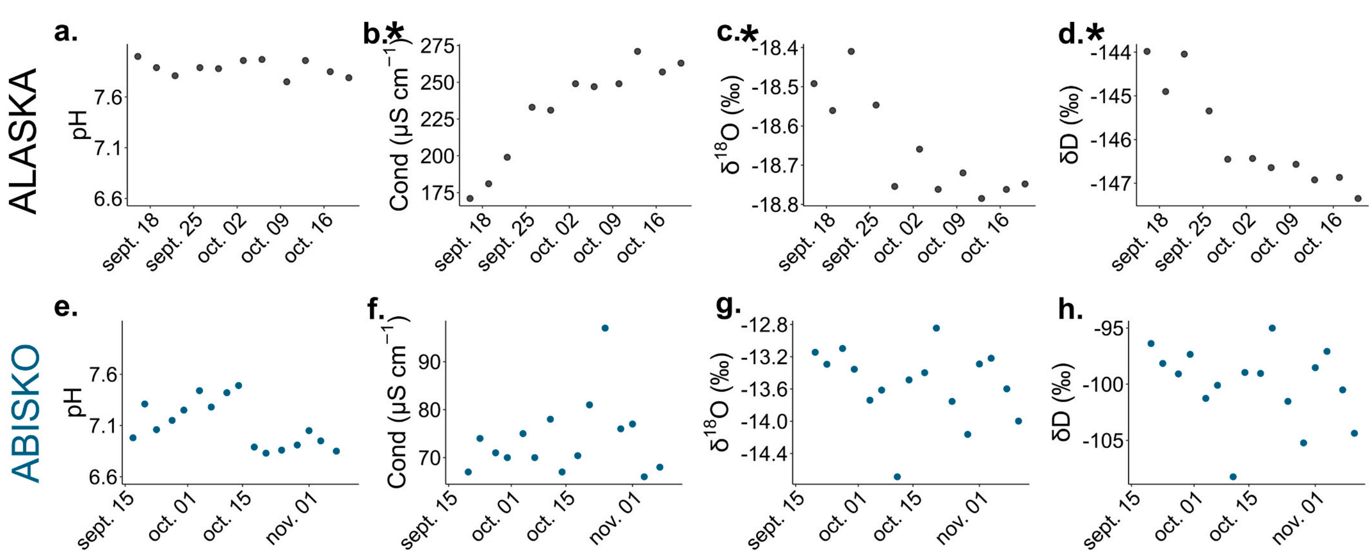

Fig. 3. pH, conductivity (Cond; in μS cm^{-1}), $\delta^{18}O$ (in ‰), and δD (in ‰) measured in the river waters from Alaska (in black; **a-d**; $n = 11$) and from Abisko (in blue; **e-h**; $n = 17$). Mann-Kendall test was performed to identify significant temporal trends (* if ***p***-value <0.05; Tables S1-S2). pH and conductivity from Abisko were published in Villani et al. (2025).

2023). Furthermore, the cumulative effect of river water freezing progressively concentrates solutes (Fig. S4) in the remaining liquid phase, further increasing its conductivity (Chen et al., 2024; Sebaaly et al., 2025). This freeze-concentration effect operates through expulsion of dissolved ions from the ice crystal lattice into residual liquid microenvironments, where solute concentrations can reach several hundred times those of the initial solution, further enhancing mineral–water interactions and reactive solute mobilization (Chen et al., 2026). These results support a closure of the soil pore water - river hydrological connectivity, as colder air and river water temperatures (Fig. 2a,b) lead to freezing processes. Here, river inputs shift from contributions of both shallow organic-rich soil pore waters and deep groundwater to increasingly mineral-rich deep groundwater-dominated flow over the late shoulder season (O'Donnell et al., 2012; Olid et al., 2022; Walvoord and Kurylyk, 2016).

In river waters from Abisko, pH values, conductivity, $\delta^{18}O$, and δD are 7.11 ± 0.23, 73 ± 8 μS cm^{-1}, −13.54 ± 0.46‰, and − 100.05 ± 3.47‰ respectively (Fig. 3e-h; Table S2). Unlike rivers in Alaska, there are no significant changes in pH, conductivity, or water isotopes over the late shoulder season in Abisko (Mann-Kendall test; *p*-value >0.05; Table S2). These results indicate that soil pore water - river hydrological connectivity persists over the late shoulder season, extending patterns previously documented during the summer period (Rocher-Ros et al., 2019). Moreover, episodic air temperatures above 0 °C when snow accumulates (Fig. 2c), leading to surface snowmelt and meltwater infiltration into soils (Villani et al., 2025), further sustain this connectivity beyond what is typically expected in late autumn conditions. However, the low variability observed at this site should also be considered in light of its particular hydrological setting as a near-stagnant river (Olefeldt and Roulet, 2012). This slow water discharge likely dampens the amplitude of seasonal variations in these chemical parameters (Liu and Wang, 2022). Moreover, the near-flat gradient of the lower catchment limits the potential contribution of deep groundwater to the river (Shogren et al., 2021). Under these conditions, it is primarily shallow, organic-rich soil pore water, rather than deeper groundwater, that sustains river input over the late shoulder season.

3.3. Mobility of Fe and DOC in rivers induced by hydrological connectivity

In river waters from Alaska, DOC and Fe concentrations, and the percentage of colloidal Fe are 7.8 ± 3.3 mg L^{-1}, 0.20 ± 0.18 mg L^{-1}, and 100 ± 0% respectively (Fig. 4a-c; Table S1). Moreover, Ce/Ce* ratio, Si concentration, and silicon isotopes ($\delta^{30}Si$) are 0.61 ± 0.19 (all indicating negative Ce anomalies), 6.58 ± 0.23 mg L^{-1}, and 1.40 ± 0.11‰ respectively (Fig. 5a-c). Over the late shoulder season, DOC and Fe concentrations decrease significantly by a factor of 3 and 16 respectively (Mann-Kendall test; ***p***-value <0.05; Fig. 4a,b; Table S1). This could be due to Fe and DOC aggregation driven by the seasonal increase in river water conductivity (Fig. 3b), supported by a significant increase in Ca, Mg, and Na concentrations over the late shoulder season (Fig. S4). In freshwater systems, divalent cations such as Ca^{2+} and Mg^{2+} play a dominant role in promoting aggregation of Fe and humic substances through cation bridging (Gunnars et al., 2002; Kloster et al., 2013; Tipping and Ohnstad, 1984), analogous to flocculation in estuarine environments (Jilbert et al., 2018), driven by distinct ionic mechanisms. Negative correlation between conductivity and Fe concentration (R^2 = 0.85) and between conductivity and DOC concentration (R^2 = 0.98; Fig. S5) also support the hypothesis of aggregation. We therefore suggest that the increase in conductivity promotes the aggregation of Fe and DOC, transferring them into the particulate fraction (> 0.22 μm) and explaining the significant decrease in DOC and Fe concentrations in the filtered river water (< 0.22 μm), although this interpretation remains indirect in the absence of dissolved oxygen, redox and suspended sediment measurements. However, we cannot rule out potential influence of changing precipitations regimes (Jorgenson et al., 2025). Although precipitation events remain generally low and sparse in Alaska over the late shoulder season (Fig. 2a), episodic air temperatures rising above 0 °C during this period can trigger snowmelt events even after initial snow accumulation, generating pulses of meltwater input in the river,

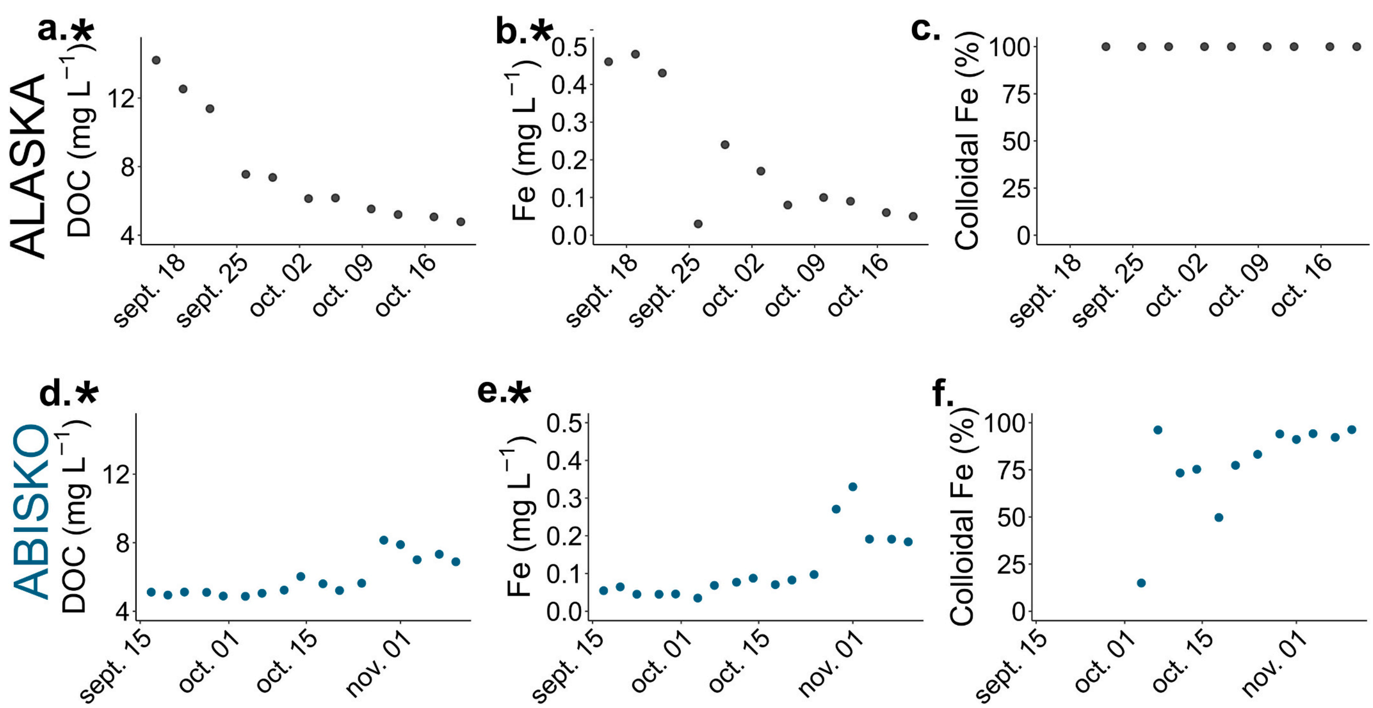

Fig. 4. DOC and Fe concentrations (in mg L^{-1}), and percentage of colloidal Fe (in %) measured in the river waters from Alaska (**a-c**; in black; *n* = 11) and from Abisko (**d-f**; in blue; *n* = 17). Some percentages of colloidal Fe were below the detection limit. Mann-Kendall test was performed to identify significant temporal trends (* if *p*-value <0.05, Tables S1-S2). Data from Abisko were published in Villani et al. (2025). (For interpretation of the references to colour in this figure legend, the reader is referred to the web version of this article.)

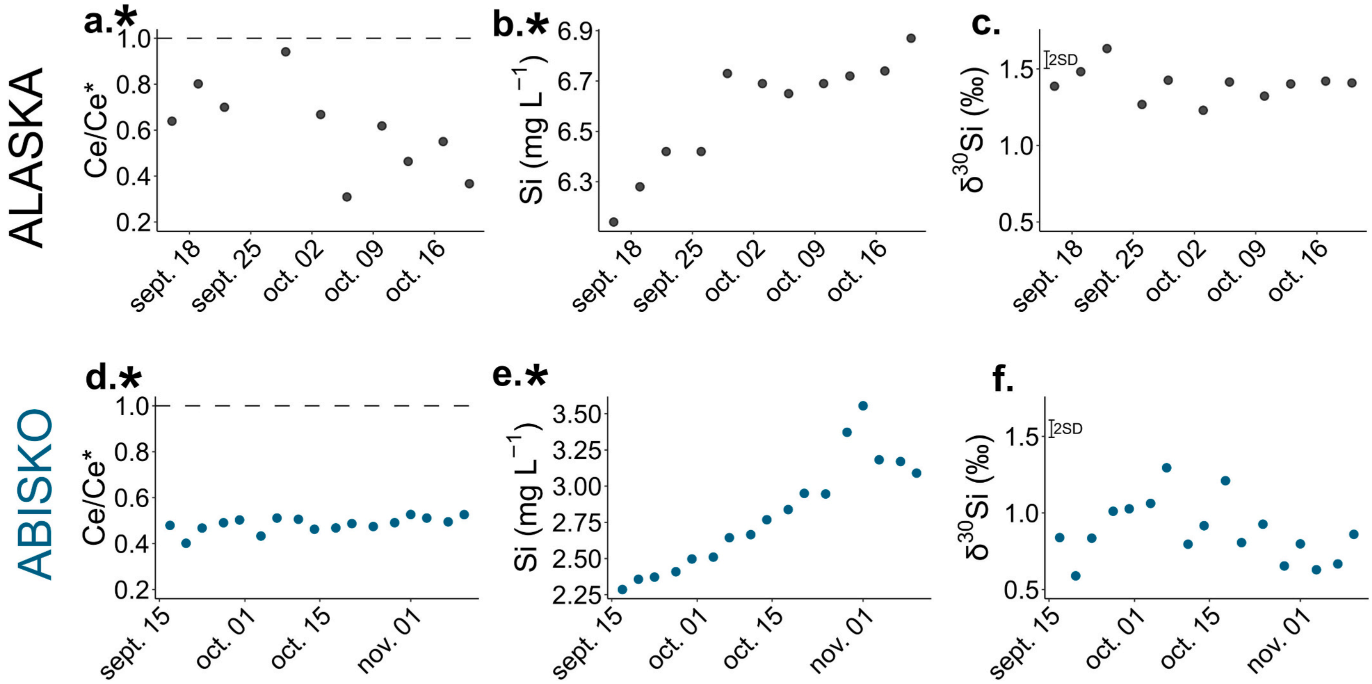

Fig. 5. Ce anomaly (Ce/Ce*), Si concentration (in mg L^{-1}), and $\delta^{30}Si$ (in ‰) measured in river waters from Alaska (in black; **a-c**; $n = 11$), and from Abisko (in blue; **d-f**; $n = 17$). Mann-Kendall test was performed to identify significant temporal trends (* if p-value <0.05; Tables S1-S2). The error bars (c,f) correspond to the standard deviation for silicon isotope measurements (2SD). Concentration in Si and $\delta^{30}Si$ from Abisko were published in Villani et al. (2025). (For interpretation of the references to colour in this figure legend, the reader is referred to the web version of this article.)

with Fe and DOC dilution (Villani et al., 2025). The persistent occurrence of colloidal Fe throughout the sampling campaign (Fig. 4c) suggests that the potential aggregation of Fe into the particulate fraction is not complete, as a residual colloidal fraction remains in the river water despite the progressive increase in conductivity driven by groundwater inputs. In addition, the significant decrease in Ce/Ce* ratio from 0.94 to 0.31 (***p***-value <0.05; Fig. 5a; Table S1) supports that Fe is present as particulate Fe-oxides: as Ce is adsorbed onto Fe-oxide surfaces (Fig. S6–7; Pourret et al., 2008, 2009), its removal into the particulate phase (> 0.22 μm) produces a higher negative Ce anomaly in the filtered fraction (< 0.22 μm). The presence of Fe-oxides is also supported by the pH conditions in the river (7.88 ± 0.08; Fig. 3a). Finally, the absence of significant variability in riverine $\delta^{30}Si$ (Fig. 5c) suggests that Si adsorption onto particulate Fe-oxides is not quantitatively significant enough to fractionate dissolved Si isotopes (Delstanche et al., 2009; Opfergelt et al., 2009). As groundwater inputs are dominant over the late shoulder season in the river in Alaska (see Section 3.2), the increase in conductivity suggests the aggregation of Fe-oxides into the particulate fraction (> 0.22 μm), likely associated with DOC given their parallel decrease (Fig. 6a).

In river waters from Abisko, DOC and Fe concentrations, and the percentage of colloidal Fe are 5.9 ± 1.1 mg L^{-1}, 0.11 ± 0.09 mg L^{-1}, and 78 ± 24% respectively (Fig. 4d-f; Table S2). Moreover, Ce/Ce* ratio, Si concentration, and silicon isotopes ($\delta^{30}Si$) are 0.48 ± 0.03 (all indicating negative Ce anomalies), 2.80 ± 0.38 mg L^{-1}, and 0.88 ± 0.20‰ respectively (Fig. 5d-f). The highly negative Ce anomaly at the beginning of the late shoulder season in Abisko likely reflects the contribution of groundwater sources, as the Ce anomaly in boreal streams is sensitive to the degree of oxidation along groundwater flow paths (Conrad et al., 2024). At the beginning of the sampling period, Fe is predominantly present in the truly dissolved fraction (< 1 nm) rather than in the colloidal form (between 1 nm and 0.22 μm), consistent with the low percentage of colloidal Fe measured at that time (Fig. 4f). Unlike the river in Alaska, Fe concentrations increase significantly over the late shoulder season by a factor of 9 (Mann-Kendall test; ***p***-value <0.05; Fig. 4b; Table S2), indicating a lateral transfer of Fe from soil pore waters to the river (Aische et al., 2025; Villani et al., 2025). The significant increase in Ce/Ce* ratio over the late shoulder season by a factor of 1.25 (***p***-value <0.05; Fig. 5d; Table S2), the percentage of colloidal Fe almost 10 times higher at the end of the sampling than at the beginning (Fig. 4c), and the positive correlation between Ce/Ce* and the percentage of colloidal Fe ($R^2 = 0.68$; Fig. S8) supports that Fe is present as colloidal Fe-oxides: as Ce is adsorbed onto colloidal Fe-oxide surfaces (Fig. S6–7; Pourret et al., 2008, 2009), its enrichment into the colloidal phase produces a lower negative Ce anomaly in the filtered fraction. This progressive shift from a dissolved Fe pool toward a colloidal Fe pool over the season is consistent with an increasing transfer of soil-derived colloids to the river (Villani et al., 2025)**.** The presence of Fe-oxides is also supported by the pH conditions in the river (7.11 ± 0.23; Fig. 3e). In parallel, the significant increase in riverine Si concentration supports a progressive enrichment in Si in the river over the late shoulder season (Fig. 5e). And the slight decrease in $\delta^{30}Si$ in river water over the late shoulder season (Fig. 5f) suggest that this enrichment in Si can be partly explained by the adsorption of Si onto the newly formed colloidal Fe-oxides preferentially adsorbing the light Si isotopes (Delstanche et al., 2009; Opfergelt et al., 2009). However, the shift in $\delta^{30}Si$ in river water cannot be solely explained by the presence of Fe-oxides and also results from the transfer of light Si isotopes originating from colloidal Si in soil pore waters, as demonstrated by a previous study on the soil to river connectivity at the study site (Villani et al., 2025). The mass-balance calculation using a fractionation factor of −1.05‰ for Si adsorption onto Fe-oxides (Delstanche et al., 2009; Opfergelt et al., 2009) indicates that the observed $\delta^{30}Si$ shift of −0.11‰ is consistent with adsorption of approximately 10% of dissolved Si (~0.24 mg L^{-1}) onto newly formed Fe-oxide colloids. However, the concurrent increase in dissolved Si concentration (+0.83 mg L^{-1}) indicates a net Si input from soil pore waters that exceeds the adsorptive sink, confirming that lateral transfer of isotopically light Si from pore waters is the dominant control on the riverine $\delta^{30}Si$ signal. In addition, DOC concentrations increase significantly by a factor of 2 (***p***-value <0.05; Fig. 4d; Table S2),

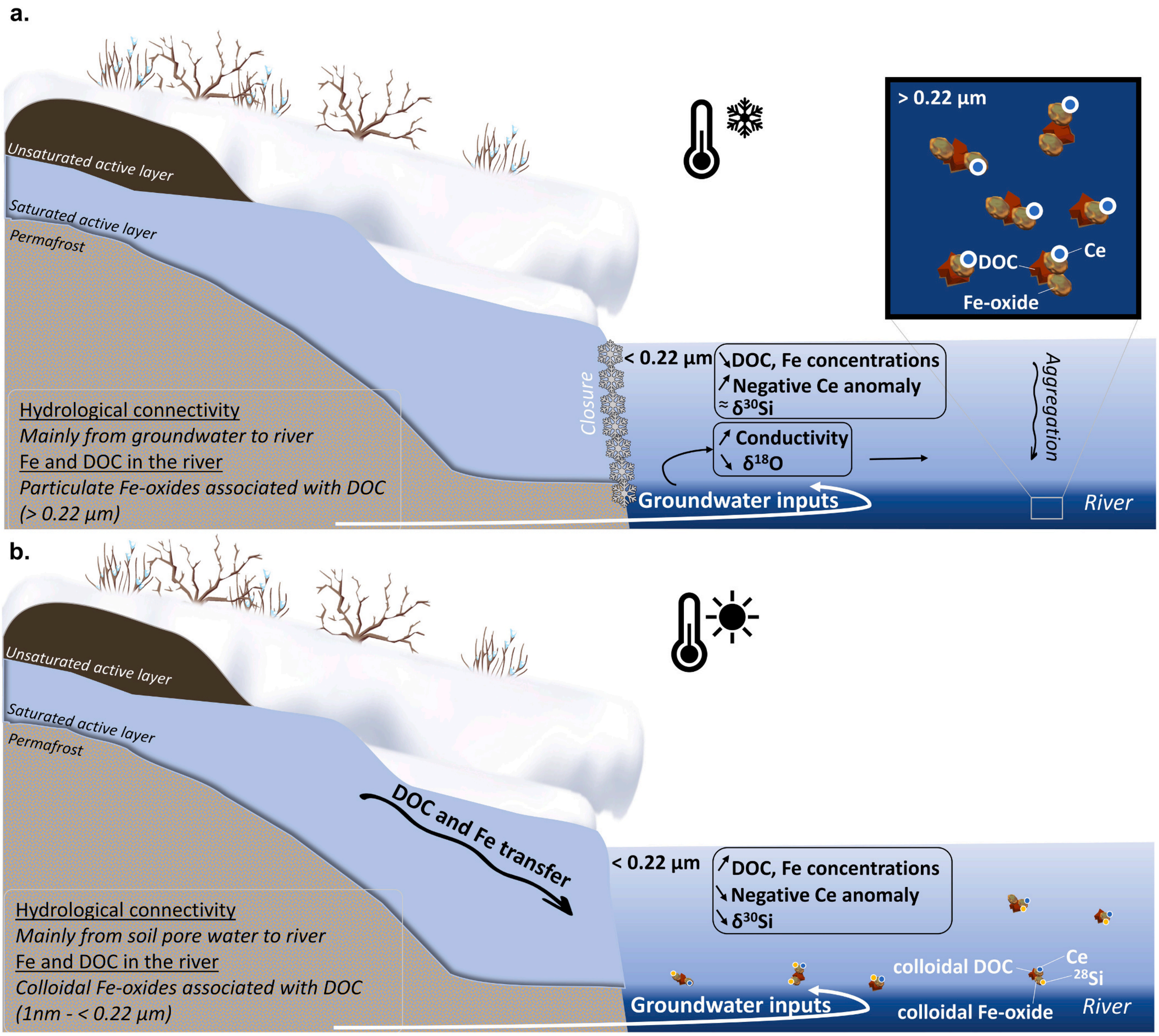

Fig. 6. Conceptual diagram illustrating the different processes occurring in rivers in Alaska (**a**) and Abisko (**b**) during the late shoulder season. The blue circles represent Ce and yellow circles represent light Si. (For interpretation of the references to colour in this figure legend, the reader is referred to the web version of this article.)

in parallel with the increase in Fe, suggesting interactions between colloidal Fe-oxides and DOC. These colloids are mainly Fe-oxides likely associated with DOC, as Fe-DOC complexes are predicted to represent a minor fraction in this river (Aische et al., 2025). As soil pore water – river connectivity persists during the late shoulder season, there is a transfer of Fe and DOC, leading to the formation of colloidal Fe-oxides likely associated with DOC, carrying Ce into the river waters (Fig. 6b). This water transfer to rivers may depend on the soil reservoirs accessed by hydrological connectivity, including frozen mineral soils (Lim et al., 2025). Frozen mineral soils can store substantial pools of Fe and DOC, including colloid-associated forms, which may be mobilized upon thaw and transferred to aquatic systems. Thus, changes in hydrological connectivity and thaw of previously frozen mineral horizons may contribute to the seasonal mobilization of Fe and DOC observed in Abisko.

3.4. *Implication of Fe-oxides associated with DOC mobility in Arctic aquatic systems*

The major difference between the rivers in Alaska and Abisko is the hypothesis of the Fe size range: particulate (> 0.22 µm) in Alaska, and colloidal (1 nm - 0.22 µm) in Abisko, suggesting contrasting size ranges of Fe-oxides likely associated with DOC. This size range suggested from our observations is consistent with the broader patterns documented across permafrost gradients in western Siberian rivers, where Fe is predominantly present in colloidal forms in permafrost-bearing rivers, with season and latitude exerting stronger control on colloidal speciation than watershed size for example (Krickov et al., 2019).

In the discontinuous permafrost region (Alaska), colder and free-flowing river conditions during the late shoulder season lead to a change in hydrological connectivity with increasing deep groundwater inputs to the river. These groundwater inputs promote the formation of particulate Fe-oxides likely associated with DOC within the river itself, as conductivity increases (Fig. 6a; Gunnars et al., 2002; Kloster et al., 2013; Tipping and Ohnstad, 1984). However, this cation-driven aggregation mechanism is unlikely to act alone. The sharp decrease in DOC to very low concentrations (~4 mg L^{-1}), the more than fivefold decrease in Fe, and the concurrent intensification of the negative Ce anomaly could also reflect a shift toward a water source with inherently low DOC content, in which Fe-oxides form and aggregate with limited DOC involvement (Krickov et al., 2020; Liu et al., 2022; Stolpe et al., 2013). In addition, the concurrent decrease in air and water temperature (Fig. 2a-b) likely increases dissolved oxygen availability, further promoting Fe oxidation and particle formation (Stumm and Lee, 1961). These mechanisms are not mutually exclusive, and the observed pattern most likely results from their combined action. The potential particles formation can have important implications for Arctic carbon budgets, as particulate Fe-oxides associated with DOC may be underestimated in land-ocean DOC flux estimates, as they are not considered in the filtered river waters (< 0.22 µm; Bowen et al., 2020; Jeandel and Oelkers, 2015; Marsac et al., 2024; McClelland et al., 2016). Potential aggregation of Fe and DOC into particles within rivers may represent a previously overlooked pathway controlling the mobility and apparent magnitude of terrestrial carbon export to the Arctic Ocean (Benoit and Rozan, 1999). The mobility of these particles is influenced by the river discharge as they could sediment and remain immobile, explaining higher particles concentrations during spring flood than during the late shoulder season (Krickov et al., 2020). A projected increase in river discharge driven by permafrost thaw (Walvoord et al., 2012) could increase the mobilization of these particles during the late shoulder season, and promote their breakdown into reactive colloidal forms, which are major forms of element migration from land to Arctic Ocean (Krickov et al., 2026; Tank et al., 2012).

In the sporadic permafrost region (Abisko), warmer and near-stagnant conditions lead to the persistence of soil pore water – river connectivity over the late shoulder season. Here, we promote the transfer of Fe and DOC from soil pore waters to the river and the formation of colloidal Fe-oxides likely associated with DOC (Fig. 6b). The colloidal size range in Abisko, more mobile and reactive than particles, increases the susceptibility to microbial and photodegradation of DOC (Bowen et al., 2020; Kelley et al., 2026). The marked increase in DOC observed near early November could additionally reflect discrete thaw events mobilizing organic colloids and Fe from plant litter, debris, and upper soil horizons (Olefeldt et al., 2013), together with silicic acid released from phytoliths carrying a lighter Si isotopic signature, consistent with the concurrent decrease in riverine δ^{30}Si (Opfergelt et al., 2009; Fig. 5f). The negative Ce anomaly observed along the late shoulder season may also, in part, be influenced by the organic conditions, where enrichment of waters in organic matter is known to promote Ce removal, rather than solely reflecting adsorption onto Fe-oxide colloids (Davranche et al., 2015). Upon reaching estuarine environments, these colloids may also flocculate (Jilbert et al., 2018; Pokrovsky et al., 2014), further modifying the mobility of associated DOC before it reaches the Arctic Ocean.

4. Conclusion

Our results demonstrate that during the late shoulder season, the mobility of Fe and DOC in Arctic rivers is strongly controlled by hydrological connectivity, which itself depends on geographic (regional permafrost), climatic (air temperatures and precipitations during the sampling period) and hydrological (free-flowing or near-stagnant river) conditions. We show two contrasting processes across the discontinuous permafrost region (Alaska, USA) and the sporadic permafrost region (Abisko, Sweden):

(i) In Alaska, colder and free-flowing river conditions during the late shoulder season drive a progressive shift in hydrological connectivity, from combined soil pore water and deep groundwater inputs toward exclusively deep groundwater-dominated river inputs, as supported by water isotopes. The resulting increase in river water conductivity first promotes the formation of Fe colloids, which potentially aggregate into the particulate fraction (> 0.22 µm), evidenced by a significant decrease in Fe concentrations in the filtered river water. The significant decrease in Ce/Ce* (higher negative Ce anomaly) and neutral pH conditions in river water support the presence of particulate Fe as particulate Fe-oxides. The parallel decrease in DOC concentrations suggests that Fe and DOC interact during this aggregation process, as Fe-oxides likely associated with DOC. These particulate Fe-oxides (> 0.22 µm) likely associated with DOC are excluded from filtered river water samples and thus not captured in dissolved carbon flux estimates.

(ii) In Abisko, warmer and near-stagnant river conditions sustain soil pore water – river connectivity over the late shoulder season, enabling continuous lateral transfer of colloidal Fe (1 nm – 0.22 µm) from soil pore waters to rivers, evidenced by a significant increase in Fe concentrations. The significant increase in Ce/Ce* (lower negative Ce anomaly) and in percentage of colloidal Fe, the slight decrease in δ^{30}Si, and neutral pH conditions support the presence of Fe as colloidal Fe-oxides. The parallel increase in DOC concentrations suggests that Fe and DOC interact, as colloidal Fe-oxides associated with DOC. These colloidal forms are more mobile than particles, and their transport in rivers increases the susceptibility of DOC to microbial and photodegradation, with potential contributions to CO_2 and CH_4 emissions.

Together, these findings highlight that the size range of the Fe-oxides likely associated with DOC, potentially particulate in Alaska and colloidal in Abisko, has direct implications for the form of terrestrial carbon export to the Arctic Ocean. Future studies incorporating dissolved oxygen and redox measurements, suspended sediment (> 0.22 µm) measurements, carbon isotopic signatures of DOC (δ^{13}C), and dissolved inorganic carbon concentrations would help better constrain the reactivity and transformation pathways of Fe and DOC in Arctic rivers, and refine estimates of DOC contribution to greenhouse gas emissions during the late shoulder season.

Declaration of generative AI and AI-assisted technologies in the manuscript preparation process

During the preparation of this work the author(s) used ChatGPT in order to assist with language editing and rephrasing of specific sentences. After using this tool/service, the author(s) reviewed and edited the content as needed and take(s) full responsibility for the content of the published article.

CRediT authorship contribution statement

Maëlle Villani: Writing – review & editing, Writing – original draft, Visualization, Methodology, Investigation, Formal analysis, Conceptualization. **Catherine Hirst:** Writing – review & editing, Methodology, Formal analysis. **Eléonore du Bois d'Aische:** Writing – review & editing, Methodology, Formal analysis. **Cécile Osy:** Writing – review & editing, Methodology. **Maxime Thomas:** Writing – review & editing, Methodology. **Philippe Roux:** Writing – review & editing, Methodology, Formal analysis. **Erik Lundin:** Writing – review & editing, Methodology. **Justin Ledman:** Writing – review & editing, Methodology. **Edward A.G. Schuur:** Writing – review & editing, Methodology. **Sophie Opfergelt:** Writing – original draft, Supervision, Project administration, Methodology, Investigation, Funding acquisition, Formal analysis, Conceptualization.

Declaration of competing interest

The authors declare that they have no known competing financial interests or personal relationships that could have appeared to influence the work reported in this paper.

Acknowledgments

We would like to thank the Swedish Polar Research Secretariat, ICOS Sweden and SITES for the support of the work done at the Abisko Scientific Research Station. ICOS Sweden and SITES are supported by the Swedish Research Council. We are grateful to 'Länsstyrelsen Norrbotten' for the access to the Stordalens naturreservat. We acknowledge the support of the Center for Ecosystem Science and Society (ECOSS) for facilitating access to the study site in Alaska. We thank R. Giesler and C.-M. Mörth for helpful discussions regarding the Abisko study site. We thank the analytical platform MOCA at UCLouvain, A. Monhonval and E. Mauclet for their contribution to field sampling, and the valuable input from the LandSense team K. Van Oost, V. Vanacker, F. Jonard and S. Lambot (Action de Recherche Concertée (ARC), no. 21/26–119, funded by the Fédération Wallonie-Bruxelles (FWB)). We acknowledge funding from the European Research Council (ERC) under the European Union's Horizon 2020 research and innovation program (ERC Starting Grant, WeThaw, n°714617) to S·O, from the Fonds National de la Recherche Scientifique to S.O., M.V. and E. d.B.A. (FNRS: FC69480, FC49507, and FC54613), from BELSPO (RT/23/LIFTHAW), and from the Royal Academy of Belgium (Fonds Agathon de Potter) to M.T. We thank the editor, Oleg S. Pokrovsky, and the two anonymous reviewers for their valuable comments.

Appendix A. Supplementary data

Supplementary data to this article can be found online at https://doi.org/10.1016/j.chemgeo.2026.123707.

Data availability

Data will be made available on request.

References

Abraham, K., Opfergelt, S., Fripiat, F., Cavagna, A.-J., De Jong, J.T.M., Foley, S.F., André, L., Cardinal, D., 2008. δ30Si and δ29Si determinations on USGS BHVO-1 and BHVO-2 reference materials with a new configuration on a Nu plasma multi-collector ICP-MS. Geostand. Geoanal. Res. 32 (2), 193–202. https://doi.org/10.1111/j.1751-908X.2008.00879.x.

du Bois d'Aische, E., Jonard, F., Hirst, C., Villani, M., Thomas, M., Giesler, R., Mörth, C.-M., Lundin, E., Van Oost, K., Vanacker, V., Lambot, S., Opfergelt, S., 2025. Permafrost Thaw Drives Iron and Organic Carbon Release Into Soil Pore Water During Palsa to Degraded Palsa Transition. https://doi.org/10.1002/ppp.70018.

Åkerman, H.J., Johansson, M., 2008. Thawing permafrost and thicker active layers in sub-arctic Sweden. Permafr. Periglac. Process. 19 (3), 279–292. https://doi.org/10.1002/ppp.626.

Benoit, G., Rozan, T.F., 1999. The influence of size distribution on the particle concentration effect and trace metal partitioning in rivers. Geochim. Cosmochim. Acta 63 (1), 113–127. https://doi.org/10.1016/S0016-7037(98)00276-2.

Bowen, J.C., Ward, C.P., Kling, G.W., Cory, R.M., 2020. Arctic amplification of global warming strengthened by sunlight oxidation of permafrost carbon to CO2. Geophys. Res. Lett. 47 (12). https://doi.org/10.1029/2020GL087085 e2020GL087085.

Box, J.E., Colgan, W.T., Christensen, T.R., Schmidt, N.M., Lund, M., Parmentier, F.-J.W., Brown, R., Bhatt, U.S., Euskirchen, E.S., Romanovsky, V.E., Walsh, J.E., Overland, J. E., Wang, M., Corell, R.W., Meier, W.N., Wouters, B., Mernild, S., Mård, J., Pawlak, J., Olsen, M.S., 2019. Key indicators of Arctic climate change: 1971–2017. Environ. Res. Lett. 14 (4), 045010. https://doi.org/10.1088/1748-9326/aafc1b.

Cardinal, D., Alleman, L.Y., Jong, J. de, Ziegler, K., André, L., 2003. Isotopic composition of silicon measured by multicollector plasma source mass spectrometry in dry plasma mode. J. Anal. At. Spectrom. 18 (3), 213–218. https://doi.org/10.1039/B210109B.

Catrouillet, C., Guenet, H., Pierson-Wickmann, A.-C., Dia, A., LeCoz, M.B., Deville, S., Lenne, Q., Suko, Y., Davranche, M., 2019. Rare earth elements as tracers of active colloidal organic matter composition. Environ. Chem. 17 (2), 133–139. https://doi.org/10.1071/EN19159.

Chambers, P.A., Brown, S., Culp, J.M., Lowell, R.B., Pietroniro, A., 2000. Dissolved oxygen decline in ice-covered rivers of northern Alberta and its effects on aquatic biota. J. Aquat. Ecosyst. Stress. Recover. 8 (1), 27–38. https://doi.org/10.1023/A:1011491706666.

Chen, T., Bui Thi, T.M., Luo, T., Cheng, W., Hanna, K., Boily, J.-F., 2024. Redox-driven formation of Mn(III) in Ice. Environ. Sci. Technol. 58 (34), 15194–15201. https://doi.org/10.1021/acs.est.4c03850.

Chen, T., Luo, T., Bui Thi, T.M., Colloc, H., Roiland, C., Le Pollès, L., Hanna, K., Boily, J.-F., 2026. Ice amplifies ligand-controlled mineral dissolution in microscale hot spots. Proc. Natl. Acad. Sci. USA 123 (17), e2532599123. https://doi.org/10.1073/pnas.2532599123.

Chupakova, A.A., Chupakov, A.V., Neverova, N.V., Shirokova, L.S., Pokrovsky, O.S., 2018. Photodegradation of river dissolved organic matter and trace metals in the largest European Arctic estuary. Sci. Total Environ. 622-623, 1343–1352. https://doi.org/10.1016/j.scitotenv.2017.12.030.

Cochand, M., Molson, J., Lemieux, J.-M., 2019. Groundwater hydrogeochemistry in permafrost regions. Permafr. Periglac. Process. 30 (2), 90–103. https://doi.org/10.1002/ppp.1998.

Conrad, S., Löfgren, S., Ingri, J., 2024. Ce anomaly in hemiboreal headwater streams: an indicator of dominant groundwater flow paths through the catchment. Ecol. Indic. 166, 112491. https://doi.org/10.1016/j.ecolind.2024.112491.

Dai, M.-H., Martin, J.-M., 1995. First data on trace metal level and behaviour in two major Arctic river-estuarine systems (Ob and Yenisey) and in the adjacent Kara Sea, Russia. Earth Planet. Sci. Lett. 131 (3), 127–141. https://doi.org/10.1016/0012-821X(95)00021-4.

Davranche, M., Gruau, G., Dia, A., Marsac, R., Pédrot, M., Pourret, O., 2015. Biogeochemical factors affecting rare earth element distribution in shallow wetland groundwater. Aquat. Geochem. 21 (2), 197–215. https://doi.org/10.1007/s10498-014-9247-6.

Davranche, M., Grau, G., Dia, A., Coz-Bouhnik, M.L., Marsac, R., Pédrot, M., Pourret, O., 2016. Rare earth elements in wetlands. In: Trace Elements in Waterlogged Soils and Sediments. CRC Press.

Delstanche, S., Opfergelt, S., Cardinal, D., Elsass, F., André, L., Delvaux, B., 2009. Silicon isotopic fractionation during adsorption of aqueous monosilicic acid onto iron oxide. Geochim. Cosmochim. Acta 73 (4), 923–934. https://doi.org/10.1016/j.gca.2008.11.014.

Diak, M., Böttcher, M.E., Ehlert von Ahn, C.M., Hong, W.-L., Kędra, M., Kotwicki, L., Koziorowska-Makuch, K., Kuliński, K., Lepland, A., Makuch, P., Sen, A., Winogradow, A., Silberberger, M.J., Szymczycha, B., 2023. Permafrost and groundwater interaction: current state and future perspective. Front. Earth Sci. 11. https://doi.org/10.3389/feart.2023.1254309.

Dial, R.J., Hanna, C.T., Sullivan, P.F., Cooper, D.J., Tino, C.J., Gregory, D.D., Diamond, C., Rieser, M., Nicolsky, D.J., Hill, K., Iwahana, G., Koch, J.C., Carey, M.P., Miller, L., Lyons, T.W., 2026. Permafrost thaw controls iron flux from wetlands and sulfide-bearing rocks to Arctic rivers and streams. Commun. Earth Environ. 7 (1), 465. https://doi.org/10.1038/s43247-026-03450-x.

Drake, T.W., Raymond, P.A., Spencer, R.G.M., 2018. Terrestrial carbon inputs to inland waters: a current synthesis of estimates and uncertainty. Limnol. Oceanogr. Lett. 3 (3), 132–142. https://doi.org/10.1002/lol2.10055.

Georg, R.B., Reynolds, B.C., Frank, M., Halliday, A.N., 2006. New sample preparation techniques for the determination of Si isotopic compositions using MC-ICPMS. Chem. Geol. 235 (1), 95–104. https://doi.org/10.1016/j.chemgeo.2006.06.006.

Grunert, B.K., Tzortziou, M., Neale, P., Menendez, A., Hernes, P., 2021. DOM degradation by light and microbes along the Yukon River-coastal ocean continuum. Sci. Rep. 11 (1), 10236. https://doi.org/10.1038/s41598-021-89327-9.

Gunnars, A., Blomqvist, S., Johansson, P., Andersson, C., 2002. Formation of Fe(III) oxyhydroxide colloids in freshwater and brackish seawater, with incorporation of phosphate and calcium. Geochim. Cosmochim. Acta 66 (5), 745–758. https://doi.org/10.1016/S0016-7037(01)00818-3.

Hirst, C., Andersson, P.S., Shaw, S., Burke, I.T., Kutscher, L., Murphy, M.J., Maximov, T., Pokrovsky, O.S., Mörth, C.-M., Porcelli, D., 2017. Characterisation of Fe-bearing particles and colloids in the Lena River basin, NE Russia. Geochim. Cosmochim. Acta 213, 553–573. https://doi.org/10.1016/j.gca.2017.07.012.

Hirst, C., Mauclet, E., Monhonval, A., Tihon, E., Ledman, J., Schuur, Edward.A.G., Opfergelt, S., 2022. Seasonal changes in hydrology and permafrost degradation control mineral element-bound DOC transport from permafrost soils to streams. Glob. Biogeochem. Cycles. https://doi.org/10.1029/2021GB007105.

Hirst, C., Andersson, P.S., Mörth, C.-M., Murphy, M.J., Schmitt, M., Kooijman, E., Kutscher, L., Petrov, R., Maximov, T., Porcelli, D., 2023a. Iron isotopes reveal seasonal variations in the mechanisms for iron-bearing particle and colloid formation in the Lena River catchment, NE Siberia. Geochim. Cosmochim. Acta 363, 77–93. https://doi.org/10.1016/j.gca.2023.09.016.

Hirst, C., Monhonval, A., Mauclet, E., Thomas, M., Villani, M., Ledman, J., Schuur, E.A. G., Opfergelt, S., 2023b. Evidence for late winter biogeochemical connectivity in permafrost soils. Commun. Earth Environ. 4 (1), 1. https://doi.org/10.1038/s43247-023-00740-6.

Hugelius, G., Strauss, J., Zubrzycki, S., Harden, J.W., Schuur, E.A.G., Ping, C.-L., Schirrmeister, L., Grosse, G., Michaelson, G.J., Koven, C.D., O'Donnell, J.A., Elberling, B., Mishra, U., Camill, P., Yu, Z., Palmtag, J., Kuhry, P., 2014. Estimated stocks of circumpolar permafrost carbon with quantified uncertainty ranges and identified data gaps. Biogeosciences 11 (23), 6573–6593. https://doi.org/10.5194/bg-11-6573-2014.

Hughes, L., Phear, A., Nicholson, D., Pantelidou, H., Soga, K., Guthrie, P., Kidd, A., Fraser, N., 2011. Carbon dioxide from earthworks: a bottom-up approach. Proc. Inst. Civil Eng. 164 (2), 66–72. https://doi.org/10.1680/cien.2011.164.2.66.

Ilina, S.M., Drozdova, O.Yu., Lapitskiy, S.A., Alekhin, Y.V., Demin, V.V., Zavgorodnyaya, Y.A., Shirokova, L.S., Viers, J., Pokrovsky, O.S., 2014. Size fractionation and optical properties of dissolved organic matter in the continuum soil solution-bog-river and terminal lake of a boreal watershed. Org. Geochem. 66, 14–24. https://doi.org/10.1016/j.orggeochem.2013.10.008.

Jeandel, C., Oelkers, E.H., 2015. The influence of terrigenous particulate material dissolution on ocean chemistry and global element cycles. Chem. Geol. 395, 50–66. https://doi.org/10.1016/j.chemgeo.2014.12.001.
Jilbert, T., Asmala, E., Schröder, C., Tiihonen, R., Myllykangas, J.-P., Virtasalo, J.J., Kotilainen, A., Peltola, P., Ekholm, P., Hietanen, S., 2018. Impacts of flocculation on the distribution and diagenesis of iron in boreal estuarine sediments. Biogeosciences 15 (4), 1243–1271. https://doi.org/10.5194/bg-15-1243-2018.
Jorgenson, K.L., Douglas, T.A., Jorgenson, M.T., Pastick, N.J., Harms, T.K., 2025. Permafrost and rain influence summer hydrologic flowpaths in boreal catchments. Water Resour. Res. 61 (6). https://doi.org/10.1029/2024WR039024 e2024WR039024.
Juhls, B., Stedmon, C.A., Morgenstern, A., Meyer, H., Hölemann, J., Heim, B., Povazhnyi, V., Overduin, P.P., 2020. Identifying drivers of seasonality in Lena River biogeochemistry and dissolved organic matter fluxes. Front. Environ. Sci. 8. https://www.frontiersin.org/articles/10.3389/fenvs.2020.00053.
Kappler, A., Bryce, C., Mansor, M., Lueder, U., Byrne, J.M., Swanner, E.D., 2021. An evolving view on biogeochemical cycling of iron. Nat. Rev. Microbiol. 19 (6), 360–374. https://doi.org/10.1038/s41579-020-00502-7.
Kelley, A.K., Pegoraro, E., Mauritz, M., Hutchings, J.A., Natali, S., Hicks-Pries, C.E., Schuur, E.A.G., 2021. Eight Mile Lake Research Watershed, Thaw Gradient: Seasonal thaw depth 2004-2020. Bonanza Creek LTER. https://doi.org/10.6073/PASTA/BEB6635175CBCE79C9F83DDF657075EE.
Kelley, A.K., Axler, Z., Ledman, J., De La Torre, M., Ebert, C.H., Springer, A.E., Kaufman, D.S., Schuur, E.a.G., 2025. Lateral dissolved organic carbon losses represent ~10% of upland tundra carbon losses and include seasonal permafrost contributions. J. Geophys. Res. Biogeosci. 130 (11), e2025JG009067. https://doi.org/10.1029/2025JG009067.
Kelley, A.K., Hirst, C., Ebert, C.H., Axler, Z., Ledman, J., Opfergelt, S., Schuur, E.A.G., 2026. Permafrost thaw exposes old dissolved organic carbon to photo- and biodegradation. Environ. Res. Ecol. 5 (1), 015003. https://doi.org/10.1088/2752-664X/ae45af.
Kennedy, E., Celis, G., See, C., Schaedel, C., Mauritz, M., Taylor, M., Ledman, J., Natali, S., Schuur, E.A.G., 2026. Eight Mile Lake Research Watershed: Hourly Meteorological Data, 2004–2025, Bonanza Creek LTER - University of Alaska Fairbanks. BNZ:453. https://doi.org/10.6073/pasta/c1b76570a7f3d4feaef428e98970b2be.
Klaminder, J., Yoo, K., Giesler, R., 2009. Soil carbon accumulation in the dry tundra: important role played by precipitation. J. Geophys. Res. Biogeosci. 114 (G4). https://doi.org/10.1029/2009JG000947.
Kleber, M., Bourg, I.C., Coward, E.K., Hansel, C.M., Myneni, S.C.B., Nunan, N., 2021. Dynamic interactions at the mineral–organic matter interface. Nat. Rev. Earth Environ. 2 (6), 402–421. https://doi.org/10.1038/s43017-021-00162-y.
Kloster, N., Brigante, M., Zanini, G., Avena, M., 2013. Aggregation kinetics of humic acids in the presence of calcium ions. Colloids Surf. A Physicochem. Eng. Asp. 427, 76–82. https://doi.org/10.1016/j.colsurfa.2013.03.030.
Krachler, R., Jirsa, F., Ayromlou, S., 2005. Factors influencing the dissolved iron input by river water to the open ocean. Biogeosciences 2 (4), 311–315. https://doi.org/10.5194/bg-2-311-2005.
Krachler, R., Krachler, R.F., von der Kammer, F., Süphandag, A., Jirsa, F., Ayromlou, S., Hofmann, T., Keppler, B.K., 2010. Relevance of peat-draining rivers for the riverine input of dissolved iron into the ocean. Sci. Total Environ. 408 (11), 2402–2408. https://doi.org/10.1016/j.scitotenv.2010.02.018.
Krickov, I.V., Pokrovsky, O.S., Manasypov, R.M., Lim, A.G., Shirokova, L.S., Viers, J., 2019. Colloidal transport of carbon and metals by western Siberian rivers during different seasons across a permafrost gradient. Geochim. Cosmochim. Acta 265, 221–241. https://doi.org/10.1016/j.gca.2019.08.041.
Krickov, I.V., Lim, A.G., Manasypov, R.M., Loiko, S.V., Vorobyev, S.N., Shevchenko, V.P., Dara, O.M., Gordeev, V.V., Pokrovsky, O.S., 2020. Major and trace elements in suspended matter of western Siberian rivers: first assessment across permafrost zones and landscape parameters of watersheds. Geochim. Cosmochim. Acta 269, 429–450. https://doi.org/10.1016/j.gca.2019.11.005.
Krickov, I.V., Loiko, S.V., Lim, A.G., Kuzmina, D.M., Istigechev, G.I., Shirokova, L.S., Pupyshev, Y.S., Pokrovsky, O.S., 2026. Hydrological continuums across climate and permafrost gradients: spatial patterns of organic carbon, greenhouse gases, and major and trace elements. Water Res. 294, 125507. https://doi.org/10.1016/j.watres.2026.125507.
Kritzberg, E.S., Villanueva, A.B., Jung, M., Reader, H.E., 2014. Importance of boreal rivers in providing iron to marine waters. PLoS One 9 (9), e107500. https://doi.org/10.1371/journal.pone.0107500.
Lim, A.G., Loiko, S.V., Pokrovsky, O.S., 2025. Organic matter, nutrients, and colloidal trace elements in pore waters, dispersed ice and aqueous leachates from mineral soils of the permafrost region. Geoderma 463, 117562. https://doi.org/10.1016/j.geoderma.2025.117562.
Liu, S., Wang, P., 2022. Emerging solute-induced mineralization in Arctic rivers under climate warming. Sci. Total Environ. 851, 158091. https://doi.org/10.1016/j.scitotenv.2022.158091.
Liu, S., Wang, P., Huang, Q., Yu, J., Pozdniakov, S.P., Kazak, E.S., 2022. Seasonal and spatial variations in riverine DOC exports in permafrost-dominated Arctic river basins. J. Hydrol. 612, 128060. https://doi.org/10.1016/j.jhydrol.2022.128060.
Lyu, Z., Sommers, P., Schmidt, S.K., Magnani, M., Cimpoiasu, M., Kuras, O., Zhuang, Q., Oh, Y., De La Fuente, M., Cramm, M., Bradley, J.A., 2024. Seasonal dynamics of Arctic soils: capturing year-round processes in measurements and soil biogeochemical models. Earth Sci. Rev. 254, 104820. https://doi.org/10.1016/j.earscirev.2024.104820.
Marsac, R., Catrouillet, C., Pédrot, M., Benedetti, M.F., Dia, A., van Hullebusch, E.D., Davranche, M., Sivry, Y., Pierson-Wickmann, A.-C., Tharaud, M., Heberling, F., 2024. Equilibrium surface complexation modeling with metastable natural colloids: the key to predict the oxidation state distribution of trace elements? Curr. Opin. Colloid Interface Sci. 72, 101820. https://doi.org/10.1016/j.cocis.2024.101820.
McClelland, J.W., Holmes, R.M., Peterson, B.J., Raymond, P.A., Striegl, R.G., Zhulidov, A.V., Zimov, S.A., Zimov, N., Tank, S.E., Spencer, R.G.M., Staples, R., Gurtovaya, T.Y., Griffin, C.G., 2016. Particulate organic carbon and nitrogen export from major Arctic rivers. Glob. Biogeochem. Cycles 30 (5), 629–643. https://doi.org/10.1002/2015GB005351.
Mueller, M.H., Alaoui, A., Kuells, C., Leistert, H., Meusburger, K., Stumpp, C., Weiler, M., Alewell, C., 2014. Tracking water pathways in steep hillslopes by δ18O depth profiles of soil water. J. Hydrol. 519, 340–352. https://doi.org/10.1016/j.jhydrol.2014.07.031.
Mzobe, P., Berggren, M., Pilesjö, P., Lundin, E., Olefeldt, D., Roulet, N.T., Persson, A., 2018. Dissolved organic carbon in streams within a subarctic catchment analysed using a GIS/remote sensing approach. PLoS One 13 (7), e0199608. https://doi.org/10.1371/journal.pone.0199608.
Mzobe, P., Yan, Y., Berggren, M., Pilesjö, P., Olefeldt, D., Lundin, E., Roulet, N.T., Persson, A., 2020. Morphometric control on dissolved organic carbon in subarctic streams. J. Geophys. Res. Biogeosci. 125 (9), e2019JG005348. https://doi.org/10.1029/2019JG005348.
Natali, S., Schuur, E.A.G., Trucco, C., Hicks Pries, C.E., Crummer, K.G., Baron Lopez, A. F., 2011. Effects of experimental warming of air, soil and permafrost on carbon balance in Alaskan tundra. Glob. Chang. Biol. 17 (3), 1394–1407. https://doi.org/10.1111/j.1365-2486.2010.02303.x.
Natali, S., Schuur, E.A.G., Rubin, R.L., 2012. Increased plant productivity in Alaskan tundra as a result of experimental warming of soil and permafrost. J. Ecol. 100 (2), 488–498. https://doi.org/10.1111/j.1365-2745.2011.01925.x.
Natali, S.M., Watts, J.D., Rogers, B.M., Potter, S., Ludwig, S.M., Selbmann, A.-K., Sullivan, P.F., Abbott, B.W., Arndt, K.A., Birch, L., Björkman, M.P., Bloom, A.A., Celis, G., Christensen, T.R., Christiansen, C.T., Commane, R., Cooper, E.J., Crill, P., Czimczik, C., Zona, D., 2019. Large loss of CO_2 in winter observed across the northern permafrost region. Nat. Clim. Chang. 9 (11), 852–857. https://doi.org/10.1038/s41558-019-0592-8.
Obu, J., 2021. How much of the earth's surface is underlain by permafrost? J. Geophys. Res.: Earth Surf. 126 (5). https://doi.org/10.1029/2021JF006123 e2021JF006123.
Obu, J., Westermann, S., Bartsch, A., Berdnikov, N., Christiansen, H.H., Dashtseren, A., Delaloye, R., Elberling, B., Etzelmüller, B., Kholodov, A., Khomutov, A., Kääb, A., Leibman, M.O., Lewkowicz, A.G., Panda, S.K., Romanovsky, V., Way, R.G., Westergaard-Nielsen, A., Wu, T., Zou, D., 2019. Northern hemisphere permafrost map based on TTOP modelling for 2000–2016 at 1 km^2 scale. Earth Sci. Rev. 193, 299–316. https://doi.org/10.1016/j.earscirev.2019.04.023.
O'Donnell, J.A., Aiken, G.R., Walvoord, M.A., Butler, K.D., 2012. Dissolved organic matter composition of winter flow in the Yukon River basin: implications of permafrost thaw and increased groundwater discharge. Glob. Biogeochem. Cycles 26 (4). https://doi.org/10.1029/2012GB004341.
Öhlander, B., Land, M., Ingri, J., Widerlund, A., 1996. Mobility of rare earth elements during weathering of till in northern Sweden. Appl. Geochem. Environ. Geochem. 11 (1), 93–99. https://doi.org/10.1016/0883-2927(95)00044-5.
Olefeldt, D., Roulet, N.T., 2012. Effects of permafrost and hydrology on the composition and transport of dissolved organic carbon in a subarctic peatland complex. J. Geophys. Res. Biogeosci. 117 (G1). https://doi.org/10.1029/2011JG001819.
Olefeldt, D., Roulet, N., Giesler, R., Persson, A., 2013. Total waterborne carbon export and DOC composition from ten nested subarctic peatland catchments—Importance of peatland cover, groundwater influence, and inter-annual variability of precipitation patterns. Hydrol. Process. 27 (16), 2280–2294. https://doi.org/10.1002/hyp.9358.
Olid, C., Rodellas, V., Rocher-Ros, G., Garcia-Orellana, J., Diego-Feliu, M., Alorda-Kleinglass, A., Bastviken, D., Karlsson, J., 2022. Groundwater discharge as a driver of methane emissions from Arctic lakes. Nat. Commun. 13 (1), 3667. https://doi.org/10.1038/s41467-022-31219-1.
Opfergelt, S., 2020. The next generation of climate model should account for the evolution of mineral-organic interactions with permafrost thaw. Environ. Res. Lett. 15 (9), 091003. https://doi.org/10.1088/1748-9326/ab9a6d.
Opfergelt, S., de Bournonville, G., Cardinal, D., André, L., Delstanche, S., Delvaux, B., 2009. Impact of soil weathering degree on silicon isotopic fractionation during adsorption onto iron oxides in basaltic ash soils, Cameroon. Geochim. Cosmochim. Acta 73 (24), 7226–7240. https://doi.org/10.1016/j.gca.2009.09.003.
Opfergelt, S., Herndon, E., Bryce, C., Hirst, C., 2026. Iron as a driver of organic carbon fate in permafrost regions. Nat. Geosci. https://doi.org/10.1038/s41561-026-02015-z.
Osterkamp, T.E., Jorgenson, M.T., Schuur, E.a.G., Shur, Y.L., Kanevskiy, M.Z., Vogel, J. G., Tumskoy, V.E., 2009. Physical and ecological changes associated with warming permafrost and thermokarst in interior Alaska. Permafr. Periglac. Process. 20 (3), 235–256. https://doi.org/10.1002/ppp.656.
Plaza, C., Pegoraro, E., Bracho, R., Celis, G., Crummer, K.G., Hutchings, J.A., Hicks Pries, C.E., Mauritz, M., Natali, S.M., Salmon, V.G., Schädel, C., Webb, E.E., Schuur, E.A.G., 2019. Direct observation of permafrost degradation and rapid soil carbon loss in tundra. Nat. Geosci. 12 (8), 627–631. https://doi.org/10.1038/s41561-019-0387-6.
Pokrovsky, O.S., Schott, J., 2002. Iron colloids/organic matter associated transport of major and trace elements in small boreal rivers and their estuaries (NW Russia). Chem. Geol. 190 (1), 141–179. https://doi.org/10.1016/S0009-2541(02)00115-8.
Pokrovsky, O.S., Shirokova, L.S., Viers, J., Gordeev, V.V., Shevchenko, V.P., Chupakov, A.V., Vorobieva, T.Y., Candaudap, F., Causserand, C., Lanzanova, A., Zouiten, C., 2014. Fate of colloids during estuarine mixing in the Arctic. Ocean Sci. 10 (1), 107–125. https://doi.org/10.5194/os-10-107-2014.

Pourret, O., Davranche, M., Gruau, G., Dia, A., 2008. New insights into cerium anomalies in organic-rich alkaline waters. Chem. Geol. 251 (1), 120–127. https://doi.org/10.1016/j.chemgeo.2008.03.002.

Pourret, O., Gruau, G., Dia, A., Davranche, M., Molénat, J., 2009. Colloidal Control on the distribution of rare Earth elements in Shallow Groundwaters. Aquat. Geochem. 16 (1), 31. https://doi.org/10.1007/s10498-009-9069-0.

Pryer, H.V., Hawkings, J.R., Wadham, J.L., Robinson, L.F., Hendry, K.R., Hatton, J.E., Kellerman, A.M., Bertrand, S., Gill-Olivas, B., Marshall, M.G., Brooker, R.A., Daneri, G., Häussermann, V., 2020. The influence of glacial cover on riverine silicon and iron exports in Chilean Patagonia. Glob. Biogeochem. Cycles 34 (12). https://doi.org/10.1029/2020GB006611 e2020GB006611.

Putman, A.L., Fiorella, R.P., Bowen, G.J., Cai, Z., 2019. A global perspective on local meteoric water lines: meta-analytic insight into fundamental controls and practical constraints. Water Resour. Res. 55 (8), 6896–6910. https://doi.org/10.1029/2019WR025181.

Reynolds, B.C., Aggarwal, J., André, L., Baxter, D., Beucher, C., Brzezinski, M.A., Engström, E., Georg, R.B., Land, M., Leng, M.J., Opfergelt, S., Rodushkin, I., Sloane, H.J., Boorn, S.H.J.M. van den, Vroon, P.Z., Cardinal, D., 2007. An inter-laboratory comparison of Si isotope reference materials. J. Anal. At. Spectrom. 22 (5), 561–568. https://doi.org/10.1039/B616755A.

Rocher-Ros, G., Sponseller, R.A., Lidberg, W., Mörth, C.-M., Giesler, R., 2019. Landscape process domains drive patterns of CO2 evasion from river networks. Limnol. Oceanogr. Lett. 4 (4), 87–95. https://doi.org/10.1002/lol2.10108.

Roux, P., Hirst, C., Villani, M., du Bois d'Aische, E., Osy, C., Kelley, A.K., Ledman, J., Schuur, E.A.G., Opfergelt, S., 2026. Radiogenic Sr isotopes reveal extended seasonal windows of soil-river dissolved organic carbon transfer in an Arctic permafrost catchment. Chem. Geol. 712, 123427. https://doi.org/10.1016/j.chemgeo.2026.123427.

Rudnick, R.L., Gao, S., 2003. 3.01—Composition of the continental crust. In: Holland, H. D., Turekian, K.K. (Eds.), Treatise on Geochemistry. Pergamon, pp. 1–64. https://doi.org/10.1016/B0-08-043751-6/03016-4.

Schuur, E.A.G., Abbott, B.W., Commane, R., Ernakovich, J., Euskirchen, E., Hugelius, G., Grosse, G., Jones, M., Koven, C., Leshyk, V., Lawrence, D., Loranty, M.M., Mauritz, M., Olefeldt, D., Natali, S., Rodenhizer, H., Salmon, V., Schädel, C., Strauss, J., Turetsky, M., 2022. Permafrost and climate change: carbon cycle feedbacks from the warming Arctic. Annu. Rev. Environ. Resour. 47, 343–371. https://doi.org/10.1146/annurev-environ-012220-011847.

Sebaaly, A.P., van Rijn, F., Hanna, K., Boily, J.-F., 2025. Ice as a kinetic and mechanistic driver of oxalate-promoted iron oxyhydroxide dissolution. Proc. Natl. Acad. Sci. 122 (35), e2507588122. https://doi.org/10.1073/pnas.2507588122.

Selinus, O., Rundqvist, R., Johansson, P., 2001. Geokemi i Göteborgs kommun. Geological Survey of Sweden (In Swedish) Göteborgsprojektet.

Shogren, A.J., Zarnetske, J.P., Abbott, B.W., Iannucci, F., Bowden, W.B., 2020. We cannot shrug off the shoulder seasons: addressing knowledge and data gaps in an Arctic headwater. Environ. Res. Lett. 15 (10), 104027. https://doi.org/10.1088/1748-9326/ab9d3c.

Shogren, A.J., Zarnetske, J.P., Abbott, B.W., Iannucci, F., Medvedeff, A., Cairns, S., Duda, M.J., Bowden, W.B., 2021. Arctic concentration–discharge relationships for dissolved organic carbon and nitrate vary with landscape and season. Limnol. Oceanogr. 66 (S1), S197–S215. https://doi.org/10.1002/lno.11682.

SMHI (Swedish Meteorological and Hydrological Institute), 2026. Meteorological data (air temperature and precipitation) for Abisko station, 2023. https://www.smhi.se/en.

Soil Survey Staff, 1999. Soil Taxonomy: A Basic System of Soil Classification for Making and Interpreting Soil Surveys, 436. U.S. Gov. Print. Off.. https://www.nrcs.usda.gov/Internet/FSE_DOCUMENTS/nrcs142p2_051232.pdf

Stolpe, B., Guo, L., Shiller, A.M., Aiken, G.R., 2013. Abundance, size distributions and trace-element binding of organic and iron-rich nanocolloids in Alaskan rivers, as revealed by field-flow fractionation and ICP-MS. Geochim. Cosmochim. Acta 105, 221–239. https://doi.org/10.1016/j.gca.2012.11.018.

Strauss, J., Fuchs, M., Hugelius, G., Miesner, F., Nitze, I., Opfergelt, S., Schuur, E., Treat, C., Turetsky, M., Yang, Y., Grosse, G., 2025. Organic matter storage and vulnerability in the permafrost domain. In: Elias, S. (Ed.), Encyclopedia of Quaternary Science, Third edition. Elsevier, pp. 399–410. https://doi.org/10.1016/B978-0-323-99931-1.00164-1.

Stumm, W., Lee, G.F., 1961. Oxygenation of ferrous iron. Ind. Eng. Chem. 53 (2), 143–146. https://doi.org/10.1021/ie50614a030.

Sun, X., Mörth, C.-M., Porcelli, D., Kutscher, L., Hirst, C., Murphy, M.J., Maximov, T., Petrov, R.E., Humborg, C., Schmitt, M., Andersson, P.S., 2018. Stable silicon isotopic compositions of the Lena River and its tributaries: implications for silicon delivery to the Arctic Ocean. Geochim. Cosmochim. Acta 241, 120–133. https://doi.org/10.1016/j.gca.2018.08.044.

Tan, H., Wen, X., Rao, W., Bradd, J., Huang, J., 2016. Temporal variation of stable isotopes in a precipitation–groundwater system: implications for determining the mechanism of groundwater recharge in high mountain–hills of the Loess Plateau, China. Hydrol. Process. 30 (10), 1491–1505. https://doi.org/10.1002/hyp.10729.

Tananaev, N., Isaev, V., Sergeev, D., Kotov, P., Komarov, O., 2021. Hydrological connectivity in a permafrost tundra landscape near Vorkuta, North-European Arctic Russia. Hydrology 8 (3), 3. https://doi.org/10.3390/hydrology8030106.

Tank, S.E., Raymond, P.A., Striegl, R.G., McClelland, J.W., Holmes, R.M., Fiske, G.J., Peterson, B.J., 2012. A land-to-ocean perspective on the magnitude, source and implication of DIC flux from major Arctic rivers to the Arctic Ocean. Glob. Biogeochem. Cycles 26 (4). https://doi.org/10.1029/2011GB004192.

Tank, S.E., Fellman, J.B., Hood, E., Kritzberg, E.S., 2018. Beyond respiration: controls on lateral carbon fluxes across the terrestrial-aquatic interface. Limnol. Oceanogr. Lett. 3 (3), 76–88. https://doi.org/10.1002/lol2.10065.

Thomas, M., Moenaert, T., Radoux, J., Delhez, B., du Bois d'Aische, E., Villani, M., Hirst, C., Lundin, E., Jonard, F., Lambot, S., Van Oost, K., Vanacker, V., Siewert, M. B., Mörth, C.-M., Palace, M.W., Varner, R.K., Sullivan, F.B., Herrick, C., Opfergelt, S., 2025. Accelerated lowland thermokarst development revealed by UAS photogrammetric surveys in the Stordalen mire, Abisko, Sweden. EGUsphere 1–40. https://doi.org/10.5194/egusphere-2025-3788.

Tian, S., Li, D., Zhang, T., McClelland, J.W., Overeem, I., Lane, S.N., Spencer, R.G.M., Wohl, E., Sha, A., Zhao, Y., Miao, C., Ning, M., Yuan, L., Ni, J., 2026. Increasing river sediment concentration and flux across the pan-Arctic. Nat. Geosci. 19 (5), 565–572. https://doi.org/10.1038/s41561-026-01960-z.

Tipping, E., Ohnstad, M., 1984. Colloid stability of iron oxide particles from a freshwater lake. Nature 308 (5956), 266–268. https://doi.org/10.1038/308266a0.

Vasyukova, E., Pokrovsky, O.S., Viers, J., Dupré, B., 2012. New operational method of testing colloid complexation with metals in natural waters. Appl. Geochem. 27 (6), 1226–1237. https://doi.org/10.1016/j.apgeochem.2012.02.026.

Villani, M., Hirst, C., du Bois d'Aische, E., Thomas, M., Opfergelt, S., Lundin, E., Giesler, R., Mörth, C.-M., 2025. Lengthening of biogeochemical processes during winter in degraded permafrost soils. Geochem. Perspect. Lett. 34 (34), 36–42.

Vogel, J., Schuur, E.A.G., Trucco, C., Lee, H., 2009. Response of CO2 exchange in a tussock tundra ecosystem to permafrost thaw and thermokarst development. J. Geophys. Res. Biogeosci. 114 (G4). https://doi.org/10.1029/2008JG000901.

Vonk, J.E., Tank, S.E., Walvoord, M.A., 2019. Integrating hydrology and biogeochemistry across frozen landscapes. Nat. Commun. 10, 5377. https://doi.org/10.1038/s41467-019-13361-5.

Walvoord, M.A., Kurylyk, B.L., 2016. Hydrologic impacts of thawing permafrost—a review. Vadose Zone J. 15 (6). https://doi.org/10.2136/vzj2016.01.0010.

Walvoord, M.A., Voss, C.I., Wellman, T.P., 2012. Influence of permafrost distribution on groundwater flow in the context of climate-driven permafrost thaw: example from Yukon Flats Basin, Alaska, United States. Water Resour. Res. 48 (7). https://doi.org/10.1029/2011WR011595.

Walvoord, M.A., Voss, C.I., Ebel, B.A., Minsley, B.J., 2019. Development of perennial thaw zones in boreal hillslopes enhances potential mobilization of permafrost carbon. Environ. Res. Lett. 14 (1), 015003. https://doi.org/10.1088/1748-9326/aaf0cc.

Yeghicheyan, D., Carignan, J., Valladon, M., Le Coz, M.B., Cornec, F.L., Castrec-Rouelle, M., Robert, M., Aquilina, L., Aubry, E., Churlaud, C., Dia, A., Deberdt, S., Dupré, B., Freydier, R., Gruau, G., Hénin, O., de Kersabiec, A.-M., Macé, J., Marin, L., Serrat, E., 2001. A compilation of silicon and thirty one TRACE elements measured in the natural river water reference material SLRS-4 (NRC-CNRC). Geostand. Newslett. 25 (2–3), 465–474. https://doi.org/10.1111/j.1751-908X.2001.tb00617.x.